COOLING BEHAVIOR AND MECHANICAL PROPERTIES OF SOLID SOLUTION STRENGTHENED FERRITIC MATERIALS

A THESIS SUBMITTED TO
THE GRADUATE SCHOOL OF NATURAL AND APPLIED SCIENCES
OF
MIDDLE EAST TECHNICAL UNIVERSITY

BY

BEHDAD SHARIATI

IN PARTIAL FULFILLMENT OF THE REQUIREMENTS
FOR
THE DEGREE OF MASTER OF SCIENCE
IN
METALLURGICAL AND MATERIALS ENGINEERING

FEBRUARY 2022

Approval of the thesis:

COOLING BEHAVIOR AND MECHANİCAL PROPERTIES OF SOLID SOLUTION STRENGTHENED FERRITIC MATERIALS

Submitted by **BEHDAD SHARIATI** in partial fulfillment of the requirements for the degree of **Master of Science** in **Metallurgical and Materials Engineering**, **Middle East Technical University by**,

Prof. Dr. Halil Kalıpçılar
Dean, Graduate School of **Natural and Applied Sciences** _____

Prof. Dr. C. Hakan Gür
Head of the Department, **Metallurgical and Materials Eng.** _____

Assist. Prof. Dr. Ali Kalkanlı
Supervisor, **Metallurgical and Materials Eng.** _____

Examining Committee Members:

Prof. Dr. Bilgehan Ögel
Metallurgical and Materials Engineering, METU _____

Prof. Dr. Ali Kalkanlı
Metallurgical and Materials Engineering, METU _____

Prof. Dr. Mehmet Erdoğan
Metallurgical and Materials Engineering, Gazi University _____

Prof. Dr. Rıza Gürbüz
Metallurgical and Materials Engineering, METU _____

Assist. Prof. Dr. Bilge İmer
Metallurgical and Materials Engineering, METU _____

Date: 08.02.2022

I hereby declare that all information in this document has been obtained and presented in accordance with academic rules and ethical conduct. I also declare that, as required by these rules and conduct, I have fully cited and referenced all material and results that are not original to this work.

Name Last name: Behdad Shariati

Signature :

ABSTRACT

COOLING BEHAVIOR AND MECHANICAL PROPERTIES OF SOLID SOLUTION STRENGTHENED FERRITIC MATERIALS

Shariati, Behdad
Master of Science, Metallurgical and Materials Engineering
Supervisor: Prof. Dr. Ali Kalkanlı

February 2022, 54 pages

In this thesis, the mechanical properties of old generation ductile iron and new generation SSF materials were compared and investigated by observing cooling behavior. For exploring the thermal analysis, cooling curves were recorded by a temperature scanner to reveal the effect of graphite shape modification by optimum inoculation. Correlations were performed with microstructural features obtained by image analysis and cooling curve analysis. It was observed that inoculation increases the TL and prevents carbide formation in the structure. After inoculation of SSF and old generation DI with 0.5%FeSi, the difference between theoretical eutectic (1152 °C) and the maximum eutectic temperature was measured by thermal analysis. It was found that ΔT changes from 7.4 to -0.8 for SSF and from 4.7 to -0.5 for S.G alloys stand for the increase in eutectic temperature over 1152°C, which is evidence of fully graphite solidification. It was found that the tensile strength decreased from 581 MPa(S.G alloy) to 512 MPa (SSF alloy), but % elongation increased from 10.7(S.G) to 18(SSF) % due to increasing ferrite phase content which is a primary benefit and characteristic of SSF alloy. The

tensile strength of DI iron alloys produced in this work was determined to be slightly higher due to the presence of 72 % pearlite compared to 2.13 % in SSF alloys produced. Due to the fully ferritic matrix structure, a 68 % increase in elongation and a 23 % increase in yield strength of SSF alloy compared to DI were achieved in this study.

Keywords: Ductile iron, SSF, mechanical property, solid solution strengthened, cooling curves.

ÖZ

KATI ÇÖZELTİ İLE GÜÇLENDİRİLMİŞ FERRİTİK MALZEMELERİN MEKANİK ÖZELLİKLERİ VE SOĞUMA DAVRANIŞI

Shariati, Behdad
Yüksek Lisans, Metalurji ve Malzeme Mühendisliği
Tez Yöneticisi: Prof. Dr. Ali Kalkanlı

Şubat 2022, 54 Sayfa

Bu tezde, eski nesil sfero ve SSF malzemelerinin mekanik özellikleri, soğuma davranışı gözlemlenerek karşılaştırılmış ve incelenmiştir. Bu iki malzemenin mekanik özellikleri, soğuma davranışı gözlemlenerek karşılaştırılmıştır ve araştırılmıştır. Termal analizi sürecini incelemek için, optimum aşılama ile grafit şelik değişikliğinin etkisini ortaya çıkarmak için bir sıcaklık tarayıcısı tarafından soğutma eğrileri kaydedilmiştir. Görüntü analizi ve soğuma eğrisi analizi ile elde edilen mikroyapısal özellikler ile korelasyonlar yapılmıştır. Aşılamanın TL'yi arttırdığı ve yapıda karbür oluşumunu engellediği gözlemlenmiştir. SSF EN-GJS 500-14'ün %0.5 FeSi ile aşılanmasından sonra teorik ötektik (1152 °C) ile maksimum ötektik sıcaklık arasındaki fark termal analiz ile ölçülmüştür. ΔT'nin SSF için 7,4'ten -0.8'e ve SG alaşımları için 4,7'den -0.5'e değiştiği, ötektik sıcaklıkta 1152°C'nin üzerindeki artışı temsil ettiği gözlemlenmiştir, bu tamamen grafit katılaşmasının kanıtıdır. Çekme mukavemeti 581 MPa'dan (SG alaşımı) 512

MPa'ya (SSF alaşımı) düştüğü tespit edilmiştir, ancak SSF alaşımının birincil faydası ve özelliği olan artan ferrit faz içeriği nedeniyle % uzama %10,7(SG)'den %18(SSF)'ye yükseldiği gözlemlenmiştir. Bu çalışmada üretilen nodül grafit dökme demir alaşımlarının çekme mukavemeti, üretilen SSF alaşımlarında % 2.13'e kıyasla % 72 perlit varlığından dolayı biraz daha yüksek olduğu tespit edilmiştir. Bu çalışmada, tamamen ferritik matris yapısı nedeniyle, nodül grafit dökme demire kıyasla SSF alaşımın uzamasında %68'lik bir artış ve akma mukavemetinde %23'lük bir artış elde edilmiştir.

Anahtar Kelimeler: Sfero döküm, SSF, mekanik özellik, katı çözelti ile güçlendirilmiş, soğuma eğrileri.

ACKNOWLEDGMENTS

I would like to express my deepest gratitude to my supervisor Prof. Dr. Ali Kalkanlı, for their guidance, advice, criticism, encouragement, and insight throughout the research.

I would like to thank Mr. Şükrü Atilgan and Mr. Murat Yildiz, who supported me in every way in my thesis work.

I would like to express my sincere thanks to my respectful wife, who has never lost her moral support in all the works that I have experienced.

TABLE OF CONTENTS

LIST OF TABLES

LIST OF FIGURES

LIST OF ABBREVIATIONS

ABBREVIATIONS

SSF	Solid Solution Strengthened Ferritic material
DI	Ductile Iron
MPa	Mega pascal
ASTM	American Society for Testing and Materials
TL	liquidus Temperatures
%	Percentage
t	Thickness
CEV	Carbon Equivalent Temperature
SC	Saturation Degree
Mm	Millimeter
H.B.	Brinell Hardness scale
CEL	Carbon Equivalent Liquidus
TEmin	Minimum Eutectic Temperature
ΔT	1150 °C- TEmin
TS	Solidus Temperature
Gr	Gram
M	Meter
RE	Rare Earth
σ, ε	Stress-Strain

CHAPTER 1

1.1 INTRODUCTION

Even though solid solution strengthened ductile iron grades were known since the 1990s, the European EN standard that includes the modern SSF grades was published in 2011. This thesis aims to study the difference between the solidification characteristics of traditional spheroidal graphite cast irons and Solution Strengthened Ferritic or SSF cast irons.

To reveal the effect of silicon content in the microstructure and mechanical properties, critical points on the cooling curves were analyzed considering the recoalescence impact of graphite formation during solidification. The work investigates solidification characteristics by thermal analysis before and after inoculation with FeSi powder. In this thesis, the solidification curves of cast materials were obtained by assessing an industrial thermal analysis system. The graphite formation periods of both S.G and SSF irons were measured on their curves. The relations between total graphite measured and tensile test results obtained as one of the important goals in this thesis. The nodule counts measured and ferrite phase determined by image analysis were different as expected. The cooling curve information was used to determine liquidus and eutectic temperature rise after inoculation and its consequent effect on graphite precipitation time intervals.

The solution strategy for the thesis goal is exploratory as well as distinctive to generate improved strength in SSF irons as-cast with features that beat current grades. However, achieving the grades' potential for greater strength requires a complete understanding of the challenges that present standardized SSF grades confront and the characteristics that can be attained utilizing the current solution strengthening with the Si approach.

1.2 LITERATURE REVIEW

1.2.1 History Of Cast Iron

Cast irons are well-known materials containing carbon contents higher than 2.14 wt %. Generally, they contain a carbon maximum of up to 4 wt% and some other main elements such as silicon, copper, manganese, which depend on the application area or the special requirements needed using related alloy. Compared to steels, the cast irons' high carbon content or concentration makes it much easier to cast because of lower melting points and lower eutectic temperature points. Cast irons are Fe-C-Si alloys and show little ductility, so they can not easily withstand the deformation process. However, they can be easily melted and cast into complex shapes, therefore often manufactured to final dimensions. They called cast irons because casting is the best fabrication method applied to these alloys. Figure 1.1 below is a schematic representation of the Iron carbon phase diagram for different carbon content in the matrix and structure. This diagram shows the two phases of metastable iron cementite and stable iron graphite. The fundamental distinction between cast irons and steels is that cast irons have a higher carbon content than steels, with more than 2.1 wt% carbon. Before developing other microstructures, iron constantly forms entirely as austenite below this carbon concentration.

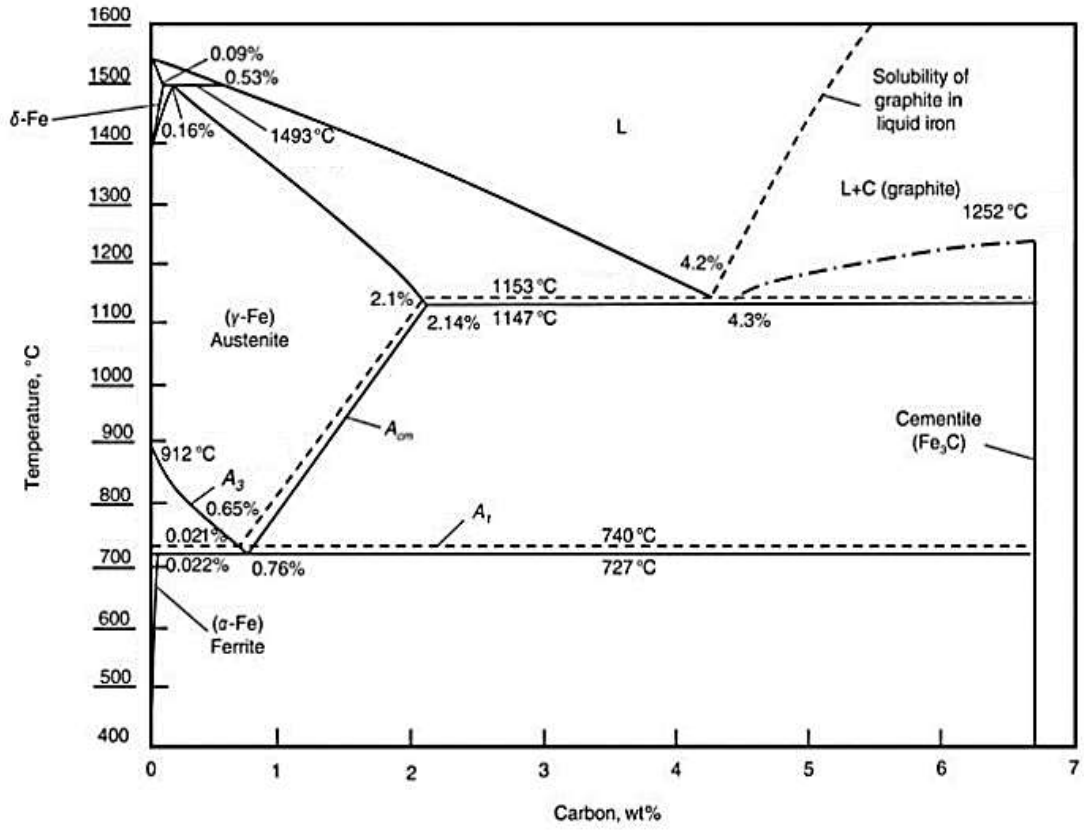

Figure1. 1: Iron-carbon phase diagram. Solid lines indicate metastable Fe-Fe3C system; dashed lines indicate stable Fe-graphite system. Adapted from [1].

1.2.2 Effect of Allying Elements

There are different types of alloying elements in cast iron. Carbon, silicon, manganese, phosphorus, and sulfur are primary elements. Some other are known as alloying elements: chromium, copper, molybdenum, and nickel. These alloying elements affect the morphology and structure of cast iron based on their amount or composition ratio inside the material and generally are pearlite promoters. In addition, Some of them, like copper and nickel, also promote graphite formation and are usually used for higher grades of ductile iron or stronger grades that need higher tensile strength. Other elements types are Trace elements like aluminum, antimony, arsenic that come from raw material as impurity and are not added

deliberately to cast iron. Common elements in cast irons and their effects are summarized in Table 1.1 below.

Table1. 1: Effect of alloying elements on the cast-iron structure. Adapted from [2].

Element	Effect on graphite formation	Effect on eutectoid reaction
Al	Strong graphitizer	Promotes ferrite
B (<0.015%)	Strong graphitizer	Promotes graphite formation
B (>0.015%)	Carbide stabilizer	Strong pearlite retainer
Bi	Carbide promoter	Very mild pearlite stabilizer
Cu	Mild graphitizer	Promotes pearlite formation
Cr	Strong carbide former	Strong pearlite former
Mn	Mild carbide former	Pearlite former
Mo	Mild carbide former	Promotes pearlite formation
Ni	Graphitizer	Mild pearlite promoter
Sb	Little effect in amount used	Strong pearlite stabilizer
Si	Strong graphitizer	Promotes ferrite and graphite formation
Sn	Little effect in amount used	Strong pearlite promoter and retainer
Te	Very strong carbide promoter	Very mild pearlite stabilizer
Ti (<0.25%)	Graphitizer	Promotes graphite formation
V	Strong carbide former	Strong pearlite former

Most of the Trace elements are pearlite and carbide promoters. However, to obtain a fully ferritic structure, the raw material or melt should be free of these elements or be as pure as possible to prevent carbide formation during solidification. As mentioned above, Some alloying elements in nodular graphite cast irons are chromium, copper, molybdenum, nickel, tin, and vanadium. Among these elements, one of the main or most important ones is magnesium. Magnesium's objective is to change the microstructure and form graphite nodules in the structure. Among these elements, nickel and copper are mainly pearlite promoters in the structure and promote graphite formation. Therefore such elements like copper are

usually used for the stronger ductile grade or where the dominant pearlitic structure is mainly needed in the matrix.

1.2.3 Graphite Morphology

Cast irons are categorized mainly into four different types based on the microstructure and metallurgical structure. Those are grey cast irons or flaky graphite cast irons, nodular graphite or ductile cast irons, White cast irons, and malleable cast irons, which are a version of the heat-treated type of White cast irons. Figur1.2 below represents the mentioned different cast irons. In grey cast iron, most of the carbon in its composition is free graphite lamellae. They are generally hyper eutectic irons containing 2.5-4% carbon content. The mechanical properties of gray cast iron are directly dependent on the casting structure and graphite morphology. It is known that, with the increase of the carbon content, the strength and hardness of the material also increase. Gray cast irons were found in many applications in engineering due to their wide variety of properties. The most important features of grey cast irons are vibration dampening ability, high strength, and cheapness or cost-effectiveness. In Nodular or ductile cast irons, carbon is in the form of graphite spheres. In order to ensure the transformation of lamellar to nodular graphite, molten iron is inoculated before casting. The graphite shape being spherical instead of lamellar gives cast iron ductility and strength. Because the graphite in gray cast iron is lamellar and has sharp corners, when the material is subjected to any stress loading, stress loading occurs at the graphite corners. Crack formation first begins in these regions, propagates, and causes a discontinuity in the matrix. Since such a phenomenon does not occur with spherical graphite, spheroidal graphite cast irons show higher strength and toughness when compared to gray cast iron of a similar structure. In white cast iron, all the carbon is available in the form of cementite (Fe_3C), which causes very high wear resistance but less fracture toughness and machinability than grey cast iron. Malleable cast irons are the heat-treated variation of white irons. At the same time, the last types are

vermicular or compacted-graphite irons which combine microstructural properties of both gray and ductile irons with worm-like or vermicular-shaped graphite [3].

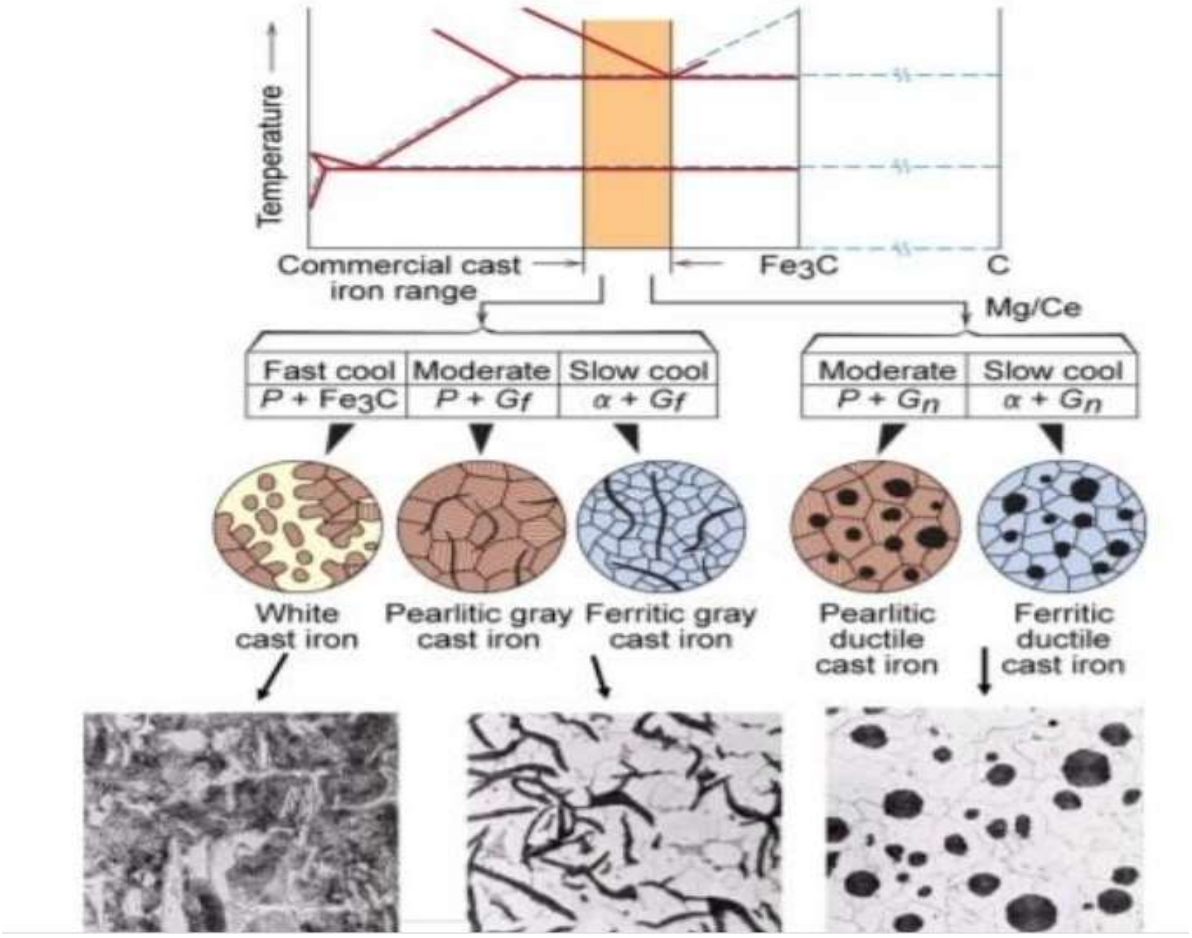

Figure1. 2: Classification of cast irons - Cooling rates and microstructures [3]

Moreover, The form of graphite particles included in cast irons is used to classify them. The EN ISO standard 945 "Microstructure of cast irons - Part 1: Graphite classification by visual analysis" specifies six distinct primary forms in cast irons, as well as various reference photos for shape and size. Figure 1.3 depicts the most common graphite shapes. Table 1.2 summarizes their descriptions, emphasizing graphite shapes seen in ductile irons.[4]

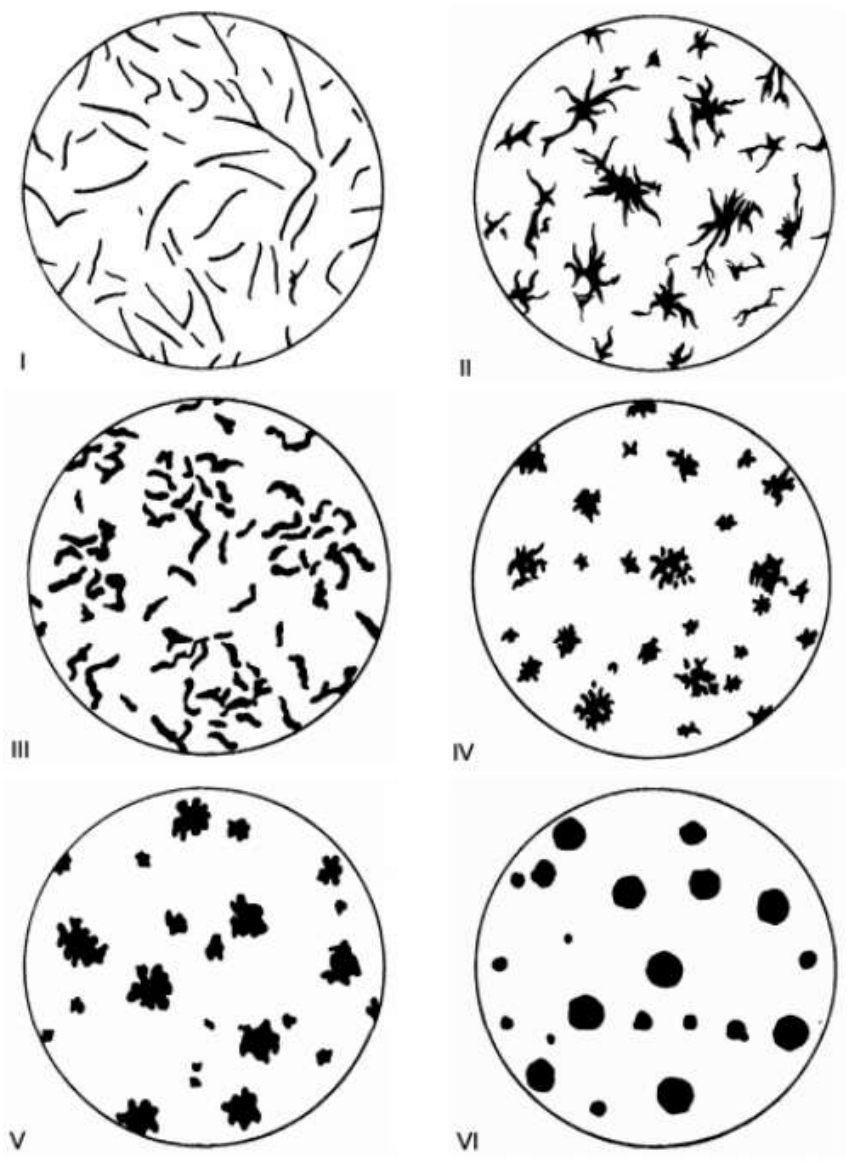

Figure1. 3: Different graphite forms according to EN 945 adopted from [4]

Table1. 2: Description of graphite forms of EN 945. Adapted from [4]

Form	Name of graphite form	Main characteristics	Occurrence
I	Lamellar (flake) graphite	Lamellar graphite with sharp ends	Principal form in gray iron
II	Crab graphite	Aggregate of graphite flakes	Can occur in rapidly cooled gray irons or thick walled ductile iron
III	Compacted graphite	Worm like with round ends	Can occur in ductile iron
IV	Irregular spheroidal graphite	Isolated particles	Can occur in ductile iron
V	Slightly irregular spheroidal graphite	Isolated particles	Principal form in thick-walled ductile iron
VI	Spheroidal graphite	Isolated particles	Principal form in ductile iron

1.2.4 Nodular Graphite/Ductile Cast Iron

Ductile irons (DI), also known as nodular or spheroidal graphite irons (SG), are made by precipitating graphite as spheroids or nodules in a liquid cast iron melt containing cerium, yttrium, or magnesium. First-generation nodular or spherical graphite cast irons were founded in the first half of the 20th century. These nodular graphite cast irons, which contain 2%-3% silicon in the matrix, are composed of ferrite, pearlite, or the mixture of these two phases. The phase ferrite has no importance alone, and by addition of dissolved carbon creates desired and requested design for different applications. Pearlite is a mixture of the carbide structure called cementite and the ferrite mentioned above. These two phases appear by lining up skinny layers within the pearlite structure. In other words, it would be more accurate to consider pearlite as a layered mixture of two phases (cementite and ferrite) rather than a single phase. Since the thin carbide layers in

the pearlite support the thin ferrite layers, this structure provides superior strength and hardness to ferrite [3]. In other words, by changing the pearlite or ferrite percent in the structure, required mechanical preppies like hardness, tensile strength, and elongation can be adjusted on produced parts based on the specific requirements. The well-known nodular graphite cast iron materials are mentioned in the European standard as EN 1563, and those are EN GJS 400-15, EN GJS 400-18, EN GJS 500-7, EN GJS 600-3, and EN GJS 700-2. Figure 1.4 represents nodular cast iron's microstructure for a) fully ferritic, b) ferritic, pearlitic matrix, and c) mainly pearlitic structures. [3]

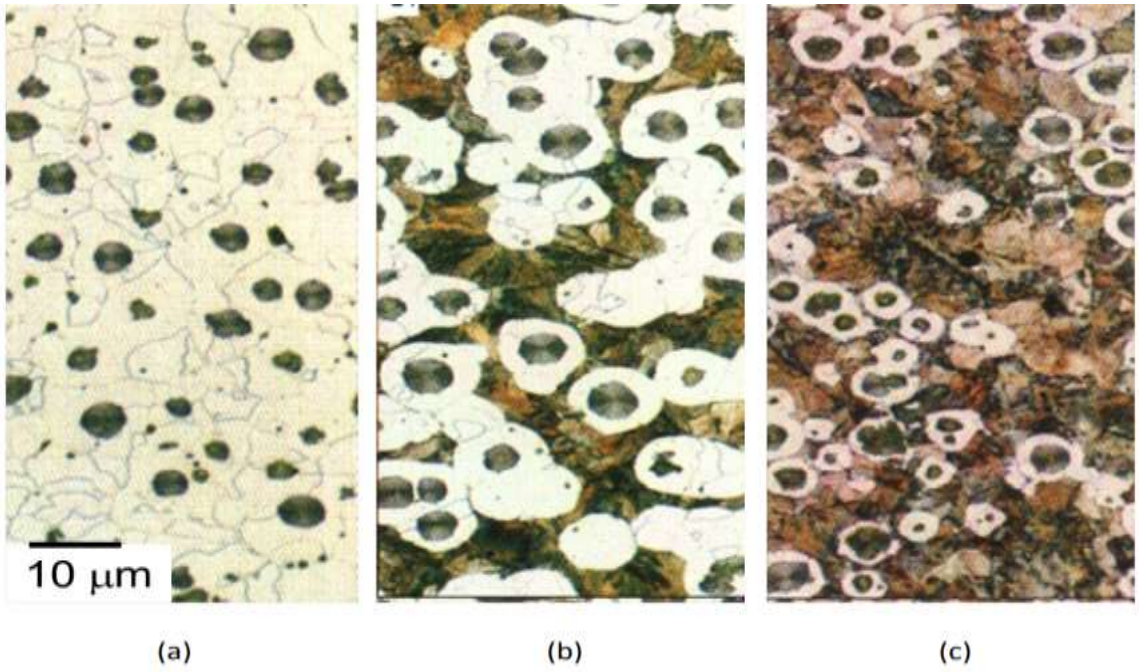

Figure1. 4: Typical microstructure of nodular cast iron, (a) Fully ferritic matrix, (b) ferritic-pearlitic matrix, (c) mainly pearlitic matrix. [3]

The desired graphite form for nodular or ductile cast iron is type VI, according to Table1.2. It is important to emphasize that the EN 1563 "Founding - Spheroidal graphite cast irons" does not necessitate obtaining this type of graphite if the mechanical properties requested for that material are satisfied after solidification. Another point is "standardized grades," which refers to the various DI classes defined by the European standard (EN standards). The "first generation ductile

irons," also known as ferritic to pearlitic grades, the "second generation ductile irons," also known as solution-strengthened ferritic (SSF) irons, both specified in the EN:1563 standard [5], and the Austempered DI (ADI) introduced in EN 1564:1997 standards, make up these DI classes. The main difference between these classes is their differing microstructures, manufacturing methods, and mechanical properties like tensile and yield strength or elongation. Based on the functionality, according to environmental conditions or load that material will expose, required grades can be produced with different mechanical properties. Table 1.3 according to EN 1563 and Table 1.4. according to EN 1564, respectively, list various irons in the ferritic to pearlitic and ADI grades. As seen in Table 1.4, increasing the grade of ductile irons means that the tensile strength and yield strength increase accordingly, and elongation decrease in higher grades. This mechanical change is because the pearlite structure increases and becomes more dominant as the grad increases. In other words, by changing the alloying element's content as copper and nickel in the melt, the morphology of cast iron changes and morphology obtained after solidification directly affect the mechanical properties [6].

Table1. 3: Mechanical properties measured on test pieces machined from cast samples for ferritic to pearlitic grades EN 1563 adopted from [5]

Material designation		Relevant wall thickness	0,2 % proof strength	Tensile strength	Elongation after fracture
		t	$R_{p0,2}$	R_m	A
		mm	MPa	MPa	%
Symbol	Number		min.	min.	min.
EN-GJS-350-22-LT [a]	5.3100	$t \leq 30$	220	350	22
		$30 < t \leq 60$	210	330	18
		$60 < t \leq 200$	200	320	15
EN-GJS-350-22-RT [b]	5.3101	$t \leq 30$	220	350	22
		$30 < t \leq 60$	220	330	18
		$60 < t \leq 200$	210	320	15
EN-GJS-350-22	5.3102	$t \leq 30$	220	350	22
		$30 < t \leq 60$	220	330	18
		$60 < t \leq 200$	210	320	15
EN-GJS-400-18-LT [a]	5.3103	$t \leq 30$	240	400	18
		$30 < t \leq 60$	230	380	15
		$60 < t \leq 200$	220	360	12
EN-GJS-400-18-RT [b]	5.3104	$t \leq 30$	250	400	18
		$30 < t \leq 60$	250	390	15
		$60 < t \leq 200$	240	370	12
EN-GJS-400-18	5.3105	$t \leq 30$	250	400	18
		$30 < t \leq 60$	250	390	15
		$60 < t \leq 200$	240	370	12
EN-GJS-400-15	5.3106	$t \leq 30$	250	400	15
		$30 < t \leq 60$	250	390	14
		$60 < t \leq 200$	240	370	11
EN-GJS-450-10	5.3107	$t \leq 30$	310	450	10
		$30 < t \leq 60$	to be agreed upon between the manufacturer and the purchaser		
		$60 < t \leq 200$			
EN-GJS-500-7	5.3200	$t \leq 30$	320	500	7
		$30 < t \leq 60$	300	450	7
		$60 < t \leq 200$	290	420	5
EN-GJS-600-3	5.3201	$t \leq 30$	370	600	3
		$30 < t \leq 60$	360	600	2
		$60 < t \leq 200$	340	550	1
EN-GJS-700-2	5.3300	$t \leq 30$	420	700	2
		$30 < t \leq 60$	400	700	2
		$60 < t \leq 200$	380	650	1
EN-GJS-800-2	5.3301	$t \leq 30$	480	800	2
		$30 < t \leq 60$	to be agreed upon between the manufacturer and the purchaser		
		$60 < t \leq 200$			
EN-GJS-900-2	5.3302	$t \leq 30$	600	900	2
		$30 < t \leq 60$	to be agreed upon between the manufacturer and the purchaser		
		$60 < t \leq 200$			

NOTE The mechanical properties of test pieces machined from cast samples can be different from the properties of the casting itself. Values for tensile properties of the casting are given in Annex B for guidance.

[a] LT for low temperature.

[b] RT for room temperature.

Table1. 4: Austempered ductile iron grades as specified in the EN 1564 adopted from [7]

Material designation		Tensile strength	0,2 % proof stress	Elongation
		R_m	$R_{p0,2}$	A
		N/mm^2	N/mm^2	%
Symbol	Number	min.	min.	min.
EN-GJS-800-8	EN-JS1100	800	500	8
EN-GJS-1000-5	EN-JS1110	1000	700	5
EN-GJS-1200-2	EN-JS1120	1200	850	2
EN-GJS-1400-1	EN-JS1130	1400	1100	1

1.2.5 Cast Iron Solidification

Depending on carbon equivalent CE, cast irons have different solidification behavior. CE contains Si, P, and C in wt% and is calculated below.

$$CE = \%C + 1\,3\,(\%Si + \%P)$$

The 4.3% carbon equivalent corresponds to the eutectic transformation at about 1150°C. The hypoeutectic, eutectic, and hypereutectic are the different solidification types of cast iron. If the CE is exactly 4.3 %, so the solidification is eutectic. If the CE is lower than 4.3, it is hypoeutectic and higher than 4.3%, and it is hypereutectic. In case the solidification behavior is hypoeutectic, iron will first solidify as primary austenite. If the solidification behavior is eutectic, a completely austenite-graphite will form, and if the solidification behaves as hypereutectic then the graphite will solidify as primer phase [9,10]. Figure 1.5 below represents the solidification process of hypereutectic cast iron with 4.5% carbon equivalent, forming the first primary graphite in the structure [8].

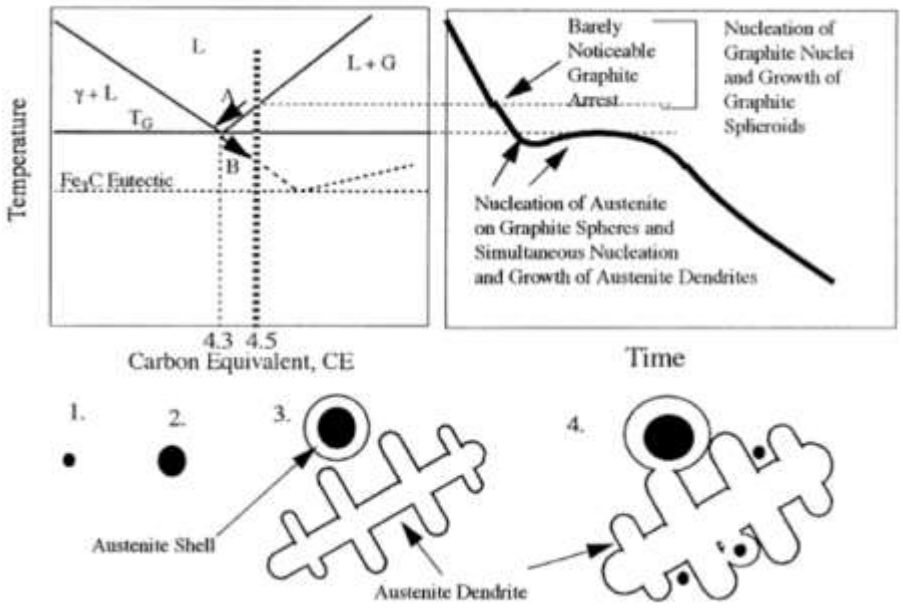

Figure1. 5: Hypereutectic solidification adopted from [11].

Stages 3 and 4 in figure 1.5 represent the formation of austenite dendrites and graphite nodules in ductile iron. The graphite nodules provide proper conditions for austenite dendrites to form around them. Moreover, melt near the nodules is depleted of carbon and cause to austenite also creates shells just around graphite [8]. Considering this solidification process, it is obvious that one of the critical factors affecting the final matrix microstructure is the chemical composition and cooling rate. Some other factors like the size, shape, and distribution of carbon particles immediately after solidification impact the casting's ultimate microstructure [8]. For example, some elements such as copper and sulfur segregate at the surface of graphite particles and function as diffusion barriers. As mentioned previously, such alloying elements are strong pearlite promoters. However, such a wall for diffusion cannot occur with other pearlite former elements like vanadium or chromium because excess levels of these elements create free intercellular carbides; hence they should be restricted in order to prevent free carbide formation [11,12].

1.3 Solid Solution Strengthened Ferritic Material

1.3.1 Strengthening Mechanism

One of the keys or main strengthening mechanisms in metals is well known as solid solution strengthening. Alloys forming solid solutions are stronger than pure metals. The reason for this phenomenon is impurity atoms which lead to strains in the surrounding matrix. In other words, these strains prevent dislocation movement and therefore result in a stronger material. Besides the increase in material strength, the ductility decreases [11]. Substitutional and interstitial atoms are the two different kinds of solute atoms. In the Interstitial, solute atoms fill the vacant space between solvent atoms, whereas solute atoms replace the solvent atoms in the substitutional. Figure 1.6 depicts the two distinct forms of solid solutions.

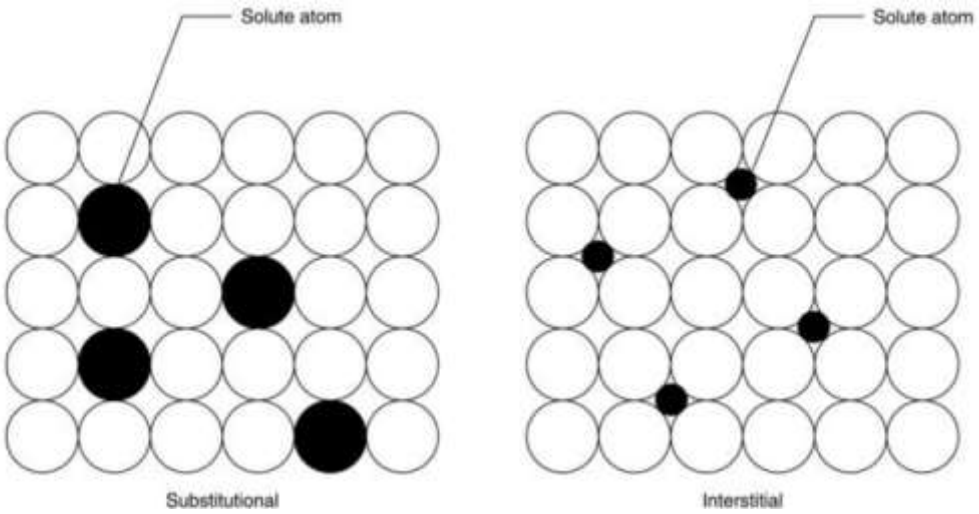

Figure1. 6: Substitutional vs. interstitial impurity atoms adopted from [11].

The impurity or solute element in solid solution strengthened ferritic materials is silicon. As previously mentioned, the element silicon promotes graphite formation. In other words, silicon supports the formation of ferrite in the process described above and prevents excessive cooling in the region. Moreover, it prevents the formation of cementite and improves the fluidity of the liquid iron. Therefore, by means of a solid solution mechanism, the material strength will increase because of limited dislocation movement. The ductility of material will be favorably improved by means of ferritic or graphite promoter element as silicon.

Furthermore, solid solution strengthening is the mechanism to determine the mechanical properties of new generation solid solution strengthening ferritic materials. This mechanism restricts the dislocation movement and prevents atomic plan shifting in the crystal lattice. When another crystal atom is placed inside the lattice, the atoms formed by a material impairs the perfection of the structure and makes it difficult for the atomic planes to slide; that is, it increases the yield strength. As a result of this event, tensile strength and yield strength increase accordingly.

1.3.2 Chemical Composition of SSF material

In addition to the above solution strengthening mechanism, The first question or concern that comes to mind is that high silicon content, which implies a more significant quantity of silicon than the first-generation alloys, provides solid solution strengthening materials with high mechanical properties and higher elongation. Why was this new generation material not found with the first-generation cast irons but created almost half a century later? When the silicon concentration of cast iron surpasses 2%, shrinkage is predicted to occur, according to a patent secured by Millis and his colleagues in 1949. According to a belief statement, mechanical properties like strength, elongation, and toughness decrease [13]. In looking for the explanation and underlying cause of what may have deceived Millis and his associates, it is clear that the cast iron alloys they studied in the patent research include 0.8 percent and above manganese (Mn). Millis and his companions were most likely fooled by the significant level of Mn in the cast irons when it came to the outcomes of the materials they made. The genuine impact of Si can be observed more clearly when the manganese level is lowered to 0.3 percent to maintain the material's elongation values high. The concept that "cast iron gets brittle as the quantity of silicon grows" sets in everyone's mind when the names include such a remark in the patent [12]. The material becomes stronger without losing too much ductility thanks to solid solution strengthening until the silicon concentration of cast iron reaches roughly 4.3 percent. When the silicon level is between 4.3 and 4.5 percent, the tensile strength and elongation values begin to decline quickly, and the material becomes brittle [6],[14], [15]. When evaluating the Si effect in SSF materials, as previously said, high silicon concentration increases yield and tensile strength. Still, when the amount of Si is raised further, the material loses strength and ductility. Figure 1.7 microstructure below, drawn from Glavas' paper, shows the harmful impact of high silicon concentration on ductility [16]. The microstructure (a) depicts the structure of the fracture surface following the tensile test of an alloy containing 3.1 % Si, as shown in the photographs.

It is evident from the fracture surface that this is a ductile fracture since dimples only exist in ductile fractures; hence it is reasonable to assume that the material has some ductility.

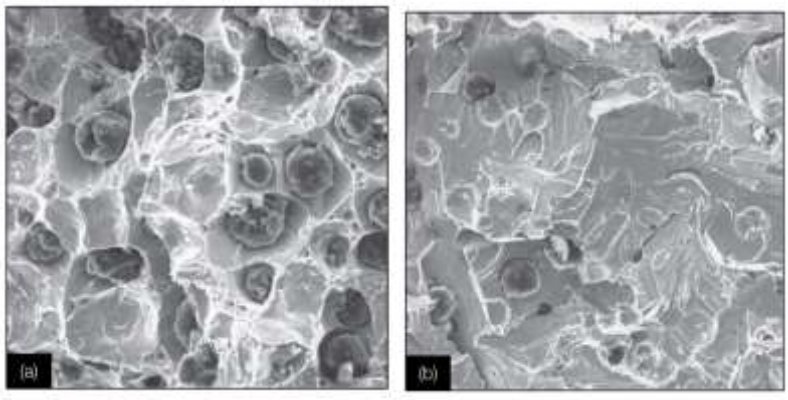

Figure1. 7: (a) Ductile fracture surface of 3.1%Si (b) Brittle fracture surface of 4.2%Si. Adopted from [16].

As previously stated, the solid solution strengthened ferrite structure, rather than pearlite, provides strength to these particular ductile cast iron alloys. Silicon elements promote graphite separation and formation. When austenite structure creates, carbon dissolution diminishes, and the carbon atom in austenite converts to graphite when the temperature decreases forms around the pro eutectic graphite. [17]. As the amount of silicon dissolved in ferrite rises, instead of the soft and weak ferrite structure we are accustomed to, ferrite structure provides enhanced strength. Furthermore, since the structure contains practically negligible pearlite, the cementite layers in the pearlite are omitted (pearlite, ferrite, and cementite). Because this brittle phase is absent from the structure, its ductility and strength are preserved, and it may display relatively high elongation values [18], [13].

Although it is mentioned that the solid solution strengthening effect is created by silicon in these new generation alloys, some different elements such as manganese and phosphorus can produce a similar effect.

Since these elements also have undesirable side effects, it is preferred to use silicon only for this study instead of these elements. For illustrate, the high content of manganese in the structure supports carbide formation, or phosphorus can lead the formation of a fragile structure called steadit. For these elements in EN 1563 standard, the recommended composition ranges are in Table 1.5 below for three main new generation materials.

Table1. 5: Summary of recommendations for solid solution composition reinforced ferritic ductile cast irons according to EN 1563. [5,18].

Material	Si%(Approx) [a]	P% (Max)	Mn%(Max)[b]
EN-GJS 450-18	3,20	0,05	0,5
EN-GJS 500-7	3,80	0,05	0,5
EN-GJS 600-10	4,30	0,05	0,5

a) Depending on the presence of different alloying elements, the %Si value can be kept lower

b) A lower manganese content (e.g., 0.30%) increases elongation and machinability.

1.3.3 Mechanical Properties of SSF Materials

Solid solution strengthened ferritic cast irons were found and developed by Volvo, Scania companies, and the Swedish Casting Institute in the early 1990s and finally entered EN 1563 in 2012 in 3 different variants which are EN GJS 450-18, EN GJS 500-14, and EN GJS 600-10 [4]. As mentioned above, the mechanical property of the final product depends on pearlite and ferrite percent in the structure. The main factor in such a structure is the chemical composition of the liquid metal. Table 1.6 below represents the three irons currently specified for the SSF grade in the EN 1563. [5], [19].

Table1. 6: Solid solid solution strengthened ferritic grades, mechanical properties measured on test pieces machined from cast samples. [5]

Material designation		Relevant wall thickness	0,2 % proof strength	Tensile strength	Elongation
		t	$R_{p0,2}$	R_m	A
		mm	MPa	MPa	%
Symbol	Number		min.	min.	min.
EN-GJS-450-18C	5.3108	$t \leq 30$	350	440	16
		$30 < t \leq 60$	340	420	12
		$60 < t \leq 200$	Guidance values to be provided by the manufacturer		
EN-GJS-500-14C	5.3109	$t \leq 30$	400	480	12
		$30 < t \leq 60$	390	460	10
		$60 < t \leq 200$	Guidance values to be provided by the manufacturer		
EN-GJS-600-10C	5.3110	$t \leq 30$	450	580	8
		$30 < t \leq 60$	430	560	6
		$60 < t \leq 200$	Guidance values to be provided by the manufacturer		

Considering the mechanical behavior of SSF materials, the most critical attitude that was brought the SSFs into greater acceptability over the ferritic to pearlitic grades was improved elongation, yield strength, and machinability. These qualities have shown to be highly important in the various applications that use SSF castings, confirming its attractiveness as a viable alternative with expanding potential and usefulness. As a result, the SSF grades were developed, which have a unique mix of intermediate strength and good ductility. Solid solution strengthening of the ferrite matrix contains roughly 3.0 - 4.4wt% Si, and the minimal amount of copper (Cu), Mn, or Tin (Sn) results in a ferritic matrix, leading to SSF irons [3], [7]. The high Si concentration also reduces the negative impact of carbide-generating components in the cast, which may be detrimental to DI characteristics. In contrast to ferritic to pearlitic grades, which rely heavily on the composite ferrite and pearlite matrix for strength, the SSF with just 5% pearlite is bolstered by the ferrite matrix. Compared to other grades, this minimum 95% ferritic structure provides a consistent hardness distribution and considerable improvements in machinability. With almost treble the elongation of ferritic to pearlitic grades, the SSFs also offer a 13-27 percent improvement in yield strength and reduced carbide formation sensitivity [4]. Solid solution strengthened ferritic materials mechanism implies that the increase of mechanical properties is not restricted to increasing the pearlite amount in the ferritic-pearlitic structure. In

other words, thanks to this new generation material and employing ferritic structure, the tensile strength improves or is the same at least level with the old generation and improves the yield strength [20], [14]. As mentioned above, it is also emphasized that there is another critical feature, different from elongation, yield strength in solid solution strengthened ductile cast irons. Figure 1.8 below shows and compare relative yield to tensile strength ratio according to tensile strength between first-generation (ferritic – pearlitic) ductile iron and new generation SSF.

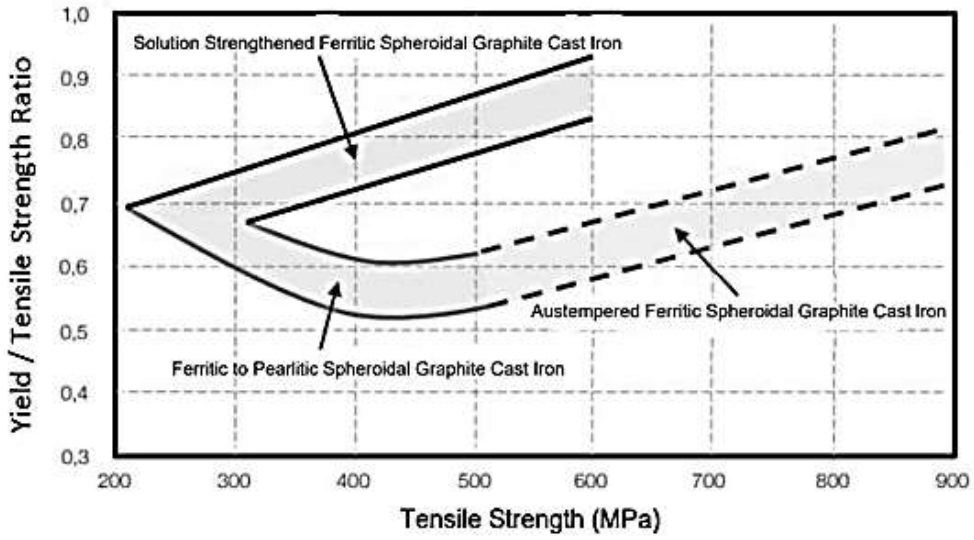

Figure1. 8: Yield/Tensile strength to Tensile strength comparison [3]

In Figure 1.8, the vertical axis shows the ratio of yield strength and tensile strength of the material. This rate increases, which means that the difference between the yield strength and tensile strength of the material is closed. For example, considering a material with a tensile strength of 600 MPa implies that the higher this ratio, the higher the yield strength. As it can be understood from the figure above, this ratio can take a maximum value of 1, and when such a situation occurs, and the balance takes the value of 1, it means that the yield and tensile strength values are equal to each other. The tensile strength of solid solution strengthened ductile cast irons is estimated to be between 450 and 600 MPa. The figure above shows the yield/tensile strength ratio is between 0.8 and 0.9,

indicating how high the materials' yield strength is. This graph shows that the ratio is approximately 0.55-0.65 in the first generation (ferritic/pearlitic) cast irons with identical tensile strength.[6,16]. Another advantage of solid solution strengthened ductile cast iron is that the hardness values remain constant regardless of section thickness. The pearlite ratio formed in SG or first-generation iron depends on the alloying elements such as copper and the material's cross-sectional thickness and cooling rate. These factors make it a big challenge to achieve a homogeneous hardness value. Figure 1.9 represents the tensile strength and hardness of SSF and first-generation iron ductile cast iron and yield strength and hardness of SSF and first-generation ductile cast iron as a) and b) respectively.

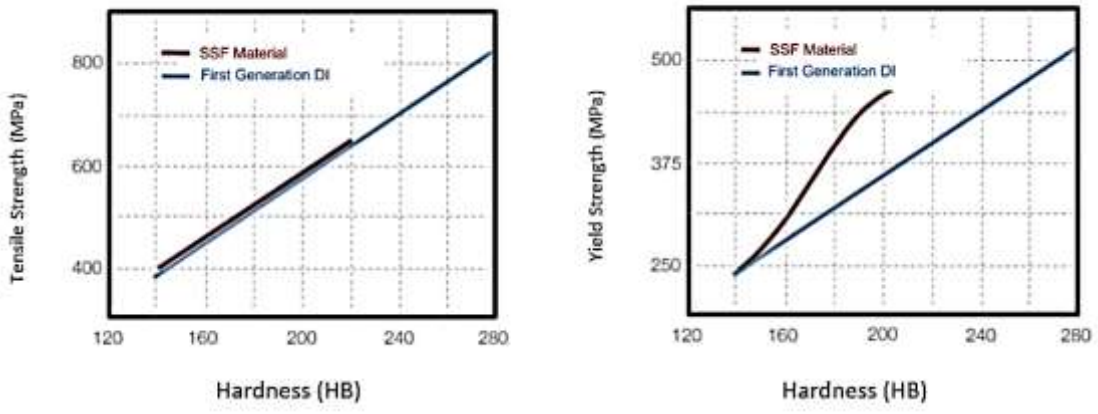

a) b)

Figure1. 9: a) Tensile strength and Brinell hardness of SSF and first-generation iron ductile cast iron b) Yield strength and Brinell hardness of SSF and first-generation. [19] .

1.3.4 Inoculation and Cooling Behavior of SSF material

Analysing the cooling of solid solution strengthened materials, the first critical issue that should be considered is that undercooling values can change with inoculation. It is mentioned that the minimum liquidus temperature (TEmin) after inoculation approaches the theoretical eutectic temperature, indicating an effect of grafting and evidence of heterogeneous nucleation. Figure 1.10 below represents

the cooling behavior of common nodular graphite cast iron recorded by thermal analysis.

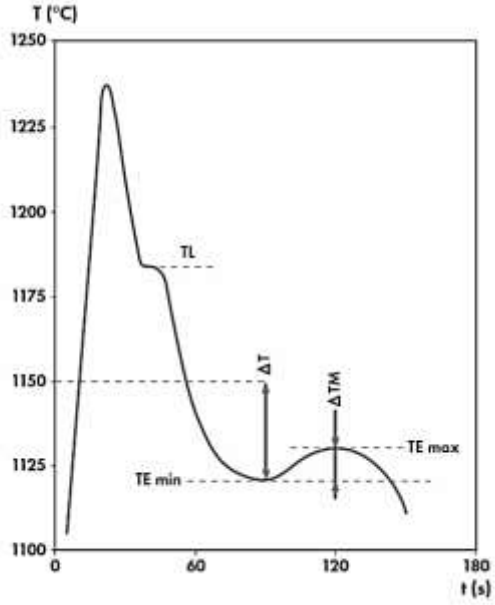

Figure1. 10: Nodular graphite cooling behavior adopted from [21].

In figure 1.10, the TL is Liquids temperature, Temin is Minimum eutectic temperature, TEmax is maximum eutectic temperature, ΔTm is the difference between TEmax and Temin, ΔT is the difference between theoretical eutectic temperature and TEmin. [26]

SSF materials are Si alloyed materials, and the addition of 75 % FeSi inoculant provides to reach and achieve much closer liquidus temperature to eutectic temperature. In other words, a high silicon ratio is desired to acquire mechanical properties requested in SSF materials, but as the excess or higher that critical amount of Si in the matrix may cause reverse results to mean brittleness. So to provide a fully ferritic structure with optimum Si amount, the FeSi inoculation help to ensure such structure through graphite formation. Increasing or decreasing solidification time lowers the undercooling that can be visible using thermal analysis [21].

Considering the real and main positive effect of inoculation, elements such as Ca, Ba, Sr, and Al in the inoculant mixture firstly combine with the free oxygen in the

liquid to form oxide inclusions. Then, Mn(x)S sulfide compound precipitates as a second layer on these oxide inclusions. These sulfide particles provide suitable surface conditions for graphite nucleation [3].

However, the efficiency of grafting mainly increases with other oxide-forming elements in the mixture. Since silicon in the inoculant is a strong graphite-former element, it facilitates the separation of graphite from the liquid. As can be understood from this explanation, there must be free oxygen and some sulfur in the liquid for the inoculation to be effective. In addition, some manganese is needed to form the sulfide compound. If the cast iron is too clean or the oxygen and sulfur levels are too low, inoculation will not be effective [21].

CHAPTER 2

EXPERIMENTAL PROCEDURE

The major goal of this thesis was to obtain more insights about EN-GJS 500-14 grade SSF ductile iron and compare the mechanical and metallurgical of these materials with first-generation ductile iron EN-GJS 500-7. Separate cast tensile U blocks were manufactured for different heat for both materials. To investigate the effect of inoculants on mechanical properties and cooling, the cooling curve of these materials was recorded and studied.

2.1 Selected alloy Type

The mechanical characteristics and cooling behavior of EN GJS 500-7, first-generation spheroidal graphite cast iron, and EN GJS 500-14, a solid solution strengthened ferritic spheroidal graphite cast iron in the new generation cast iron alloys, were investigated after a literature review.

2.1.1 Production of Samples

Samples were produced in Ekstrametal Foundry in Ankara, three tones induction furnace was prepared for this purpose. The three tones furnace photo is represented in figure 2.1.

Figure2. 1: Three tones induction furnace

The furnace charge included pig iron, steel scrap, and foundry returns (runner). The ratio for these raw materials is given in table 2.1 below.

Table2. 1: Charge material for Three tones induction furnace.

Material Name	**Pig Iron**	**Steel Scrap**	**Foundry Returns**	**Remain Allying Elements As Cu, Mn, Si ,SiC**
Content for Three Tones of Charge	**30%**	**30%**	**30%**	**balance based on the compositin of Target Material**

The charge melting time in induction furnaces was approximately 45 minutes, and melting was achieved by temperature control. Additionally, the requisite carbon, silicon, and manganese ratios and the required magnesium and crucible inoculation ratios were also calculated and added during furnace preparation. The produced materials' furnace exit temperature was about 1530°C. The nodularization procedure was carried out using a cored wire FeSiMg treatment technique, as shown in figure 2.2. The casting temperature was measured at 1380°C using thermocouple equipment. The casting time for the moulds was determined to be seven minutes, the Mg recovery for this treatment was defined as 30 %.

The cored wire main elements consist of Mg in around 25 % (62 Gr/m), Si in 44% (108 Gr/m), and RE elements as 1 % (2Gr/m).

Figure2. 2: Cored wire Mg treatment for nodular graphite cast iron.

The target composition of the furnace after Mg or nodularization heat treatment for both the first generation (EN-GJS 500-7) and the new generation (EN-GJS 500-14) was aimed as in Table 2.2 below.

Table2. 2: Target chemical analysis for EN-GJS 500-7 and EN-GJS 500-14 after Mg treatment.

Material Name	Min C %	Max C%	Min Si %	Max Si%	Min Mn %	Max Mn %	Min Mg %	Max Mg %	Min Cu%	Max Cu%
EN -GJS 500-7	3,60	3,70	2,10	2,25	0,20	0,30	0,04	0,06	0,30	0,35
EN- GJS 500-14	2,90	3,10	3,70	3,80	x	0,30	0,035	0,055	x	0,10

As seen in Table 2.2, there is a range for each element because, as mentioned previously, each has a different effect on the final microstructure.

For example, copper (Cu) is a pearlite formation element and stabilizes pearlite in the structure. Manganese (Mn) retard ferrite formation and refine lamella in the pearlite. Magnesium (Mg) is used for desulfurization and nodularization, and silicon is a graphite promoter and affects the CE, the nodule count, and matrix structure. After the heat treatment process, the inoculation process was carried out by FeSi inoculant in 0.5% amount. Adjusting the solidification time and undercooling amount are the two main advantages of inoculation. Figure 2.3 represents the ladle inoculation of heat before casting.

Figure2. 3: Ladle inoculation before pouring the melt.

Table 2.3 describes the Barinoc inoculant composition used for this purpose.

Table2. 3: Barinoc inoculant compostion

Element	**Wt%**
Si	71.12
Ba	2.45
Ca	1.50
AL	1.21
Size	1-3 mm

After the melt was prepared, the moulds and samples were produced, as shown in figure 2.4 below. The test samples were designed based on the down drawing 2.5. after that, using a universal turning machine, those samples were machined to the dimension mentioned in EN1563:2018.

Figure2. 4: U block test sample

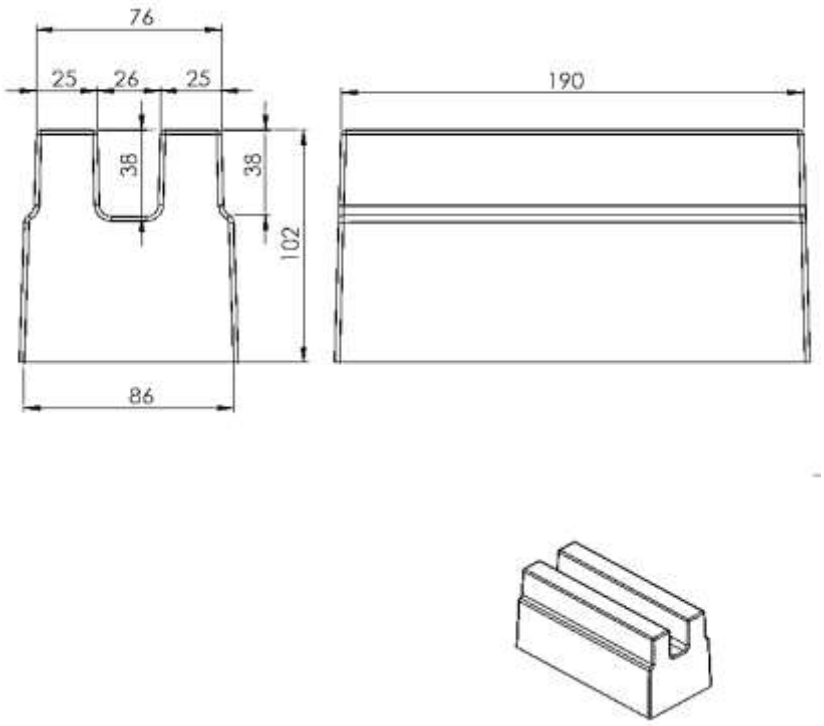

Figure2. 5: Test sample cast dimension.

2.1.2 Thermal Analysis of Cast Irons

In order to observe the cooling behavior and effect of the Si on the cooling properties of the alloys, EN-GJS500-7 and EN GJS, 500-14 were prepared and cast into analysis cups before and after inoculation and cooling curve recorded using Quik-Cup Electro-Nite thermal analysis instrument. Two different alloys were delivered into sand moulds for tensile test samples with and without 0.5 % FeSi inoculation for both materials. Figure 2.6 represents the Quick cup sampling port and resin bonded disposable cup installed.

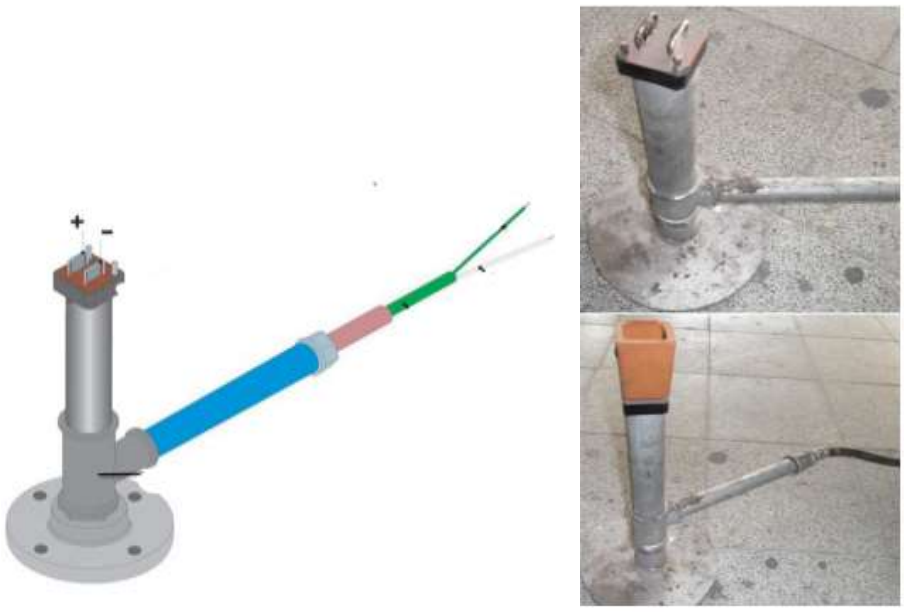

Figure2. 6: Quick up test sample port for thermal analysis.

2.1.3 Microstructural Control

A chill test and a microstructure block were taken during the casting process to check the melt chemical analysis and microstructure. Figure 2.7 a) represents a sample of chill tests for chemical analyses, figure 2.7 b) represents the sample block for microstructural examination and hardness test.

a) b)

Figure2. 7: a) Chill test for chemical analysis b) microstructural blocks for hardness test

2.1.4 Mechanical Properties (Hardness and Tensile Test)

After the tensile tests were produced in U blocks, those 12 samples were machined according to EN –ISO 6892-1 [29] Figure 2.8 below.

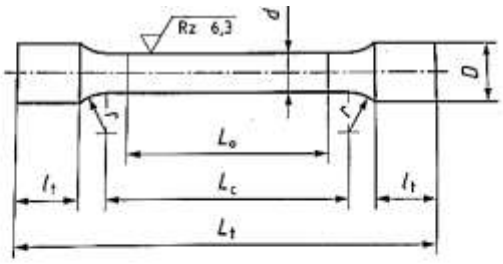

Key

d	L_o	L_c min.
5	25	30
7	35	42
10	50	60
14 [a]	70	84
20	100	120

[a] Preferred dimension for 25 mm cast sample diameter.

Figure2. 8: Standard test specimen for tensile test [19], [6].

The hardness measurement was carried out with BMS 3000 kg-OBPC with a 10 mm Brinell carbide ball. Figure 2.9 represents the hardness machine used for hardness measurement.

Figure2. 9: Hardness test instruments used for measurement.

Tensile tests were applied in the laboratory using the MTS 30 tones tensile test machine represented in figure 2.10 below.

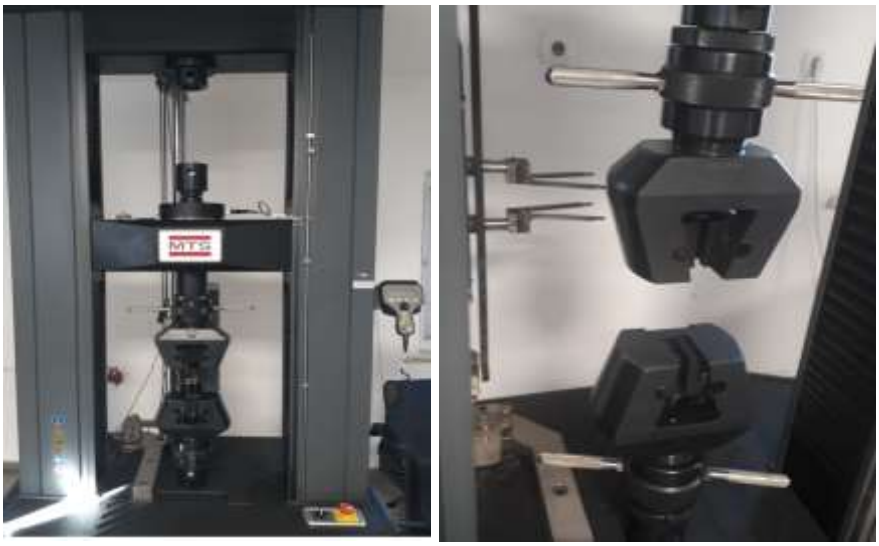

Figure2. 10: Tensile test instruments used for measurement

CHAPTER 3

EXPERIMENTAL RESULTS

3.1.1 Chemical Analysis Results

As mentioned after sample preparation, spectrometer analysis was carried out to check the percentage of the element in each alloy sample. For control, the analysis for both first-generation EN GJS 500-7 and new generation EN-GJS 500-14the the OBLF spectrometer analysis machine was used. Comparing the spectrometer results with Table 2.2, the chemical composition of both samples was in the target range, as seen in Table 3.1 below.

Table3. 1: Final chemical composition of EN-GJS 500-7 and EN-GJS 500-14 casted samples.

Material Name	**C%**	**Si %**	**Mn%**	**Mg%**	**Cu%**
EN -GJS 500-7	3,61	2,17	0,28	0,048	0,35
EN- GJS 500-14	2,95	3,79	0,16	0,041	0,05

3.1.2 Microstructural Results

The test blocks were likewise made after grinding and polishing, and the microstructure of the test samples was examined under a Nikon microscope. Figures 3.1, 3.2, and 3.3 show the microstructure of the three test samples of EN-GJS 500-7 a)before etching and b) after etching in each casting batch of three tones melt. The etching was carried out using 3% Nital Etchant.

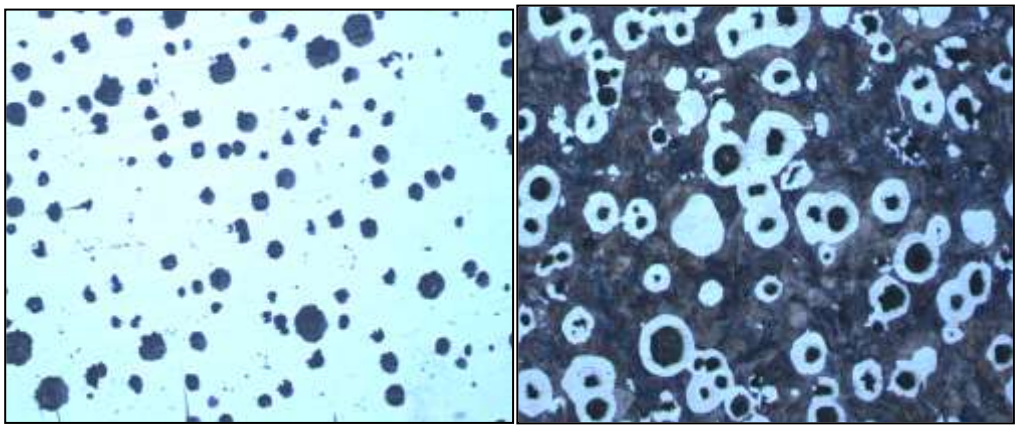

a b

Figure3. 1: sample 1 microstructure a) before etching, b) after %3 Nital etchant in 100x magnification.

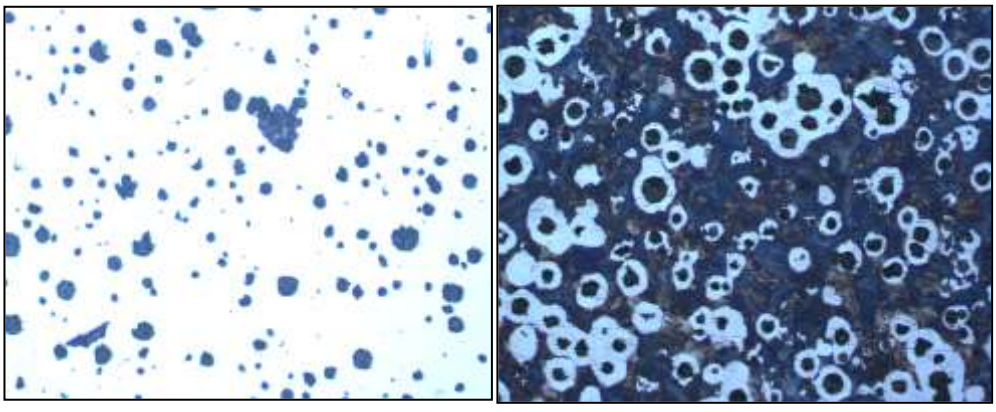

a b

Figure3. 2: sample 2 microstructure a) before etching, b) after %3 Nital etchant 50x magnification.

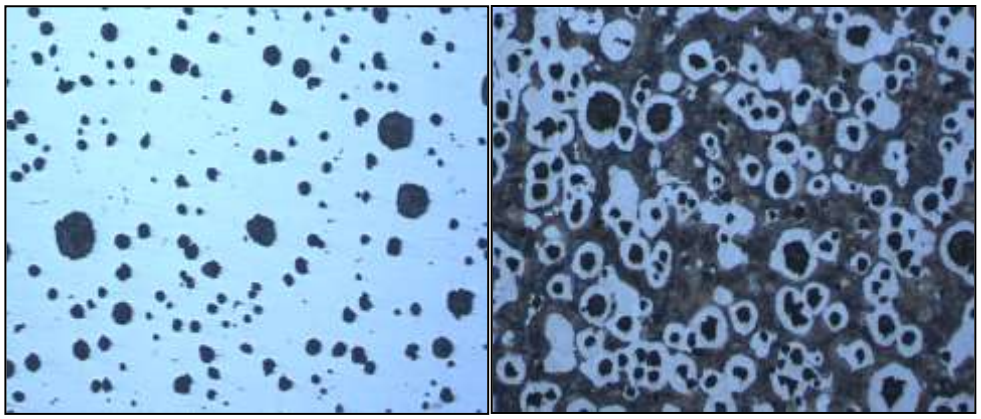

a b

Figure3. 3: sample 3 microstructure a) before etching, b) after %3 Nital etchant

50x magnification.

Figures 3.4, 3.5, and 3.6 show the microstructure of the three test samples of EN-GJS 500-14 a)before etching and b) after etching in each casting batch of three tones melt. The etching was carried out using 3% Nital Etchant.

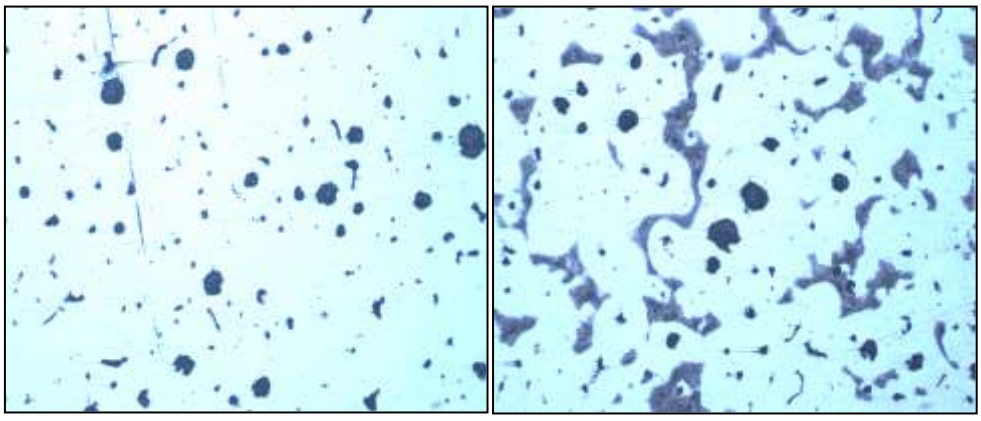

a b

Figure3. 4: Sample 1 microstructure a) before etching, b) after %3 Nital etchant in 100x magnification.

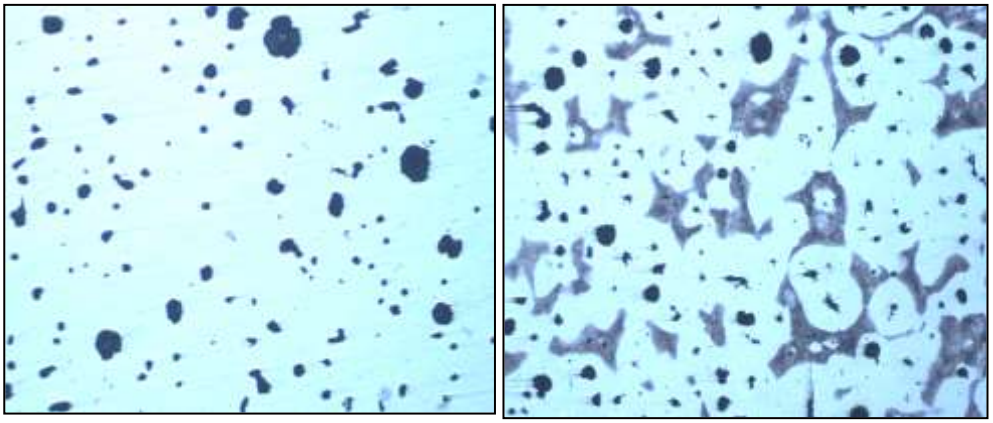

a b

Figure3. 5: Sample 2 microstructure a) before etching, b) after %3 Nital etchant in 50x magnification.

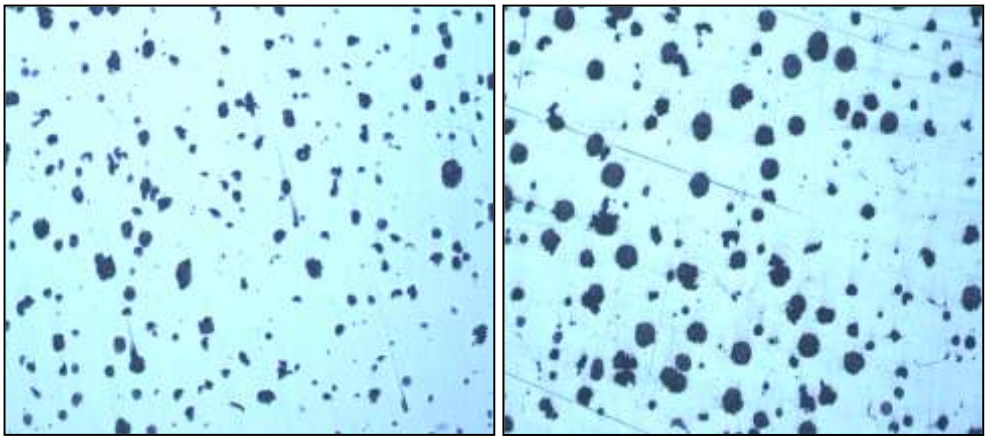

a b

Figure3. 6: Sample 3 microstructure a) before etching, b) after %3 Nital etchant in 50x magnification.

In Figures 3.1, 3.2, and 3.3 above, the black area shows the pearlite area, and the white area rounded the nodules represent ferrite. So in such materials, pearlite should be within min 60% and max 90% range. So as it is clear from the Figures above and considering the microstructure results, the pearlite amount satisfies min

amount in the structure. The new generation structure is requested to be achieved as min 95 % ferrite. As precise from Figures 3.4, 3.5, and 3.6 after etching, the structure is 95 % ferrite.

Figure 3.7 represents the EN-GJS 500-7 microstructure, and Figure 3.8 illustrates the microstructure analysis for the first and new generations EN-GJS 500-14. There is only one representative figure from each heat to show the correspondence between microstructure and the ferrite and pearlite amount. In nodular cast irons, min 170 reported in EN1563 nodules is required to be observed in the structure, and the results shown in the figure below are evidence that the nodule count for these is pretty enough.

Sample ID:	GGG50		**Nodularity by Count:**	72,19	**Graphite %:** 12,65
Fields:	3		**Nodularity by Area:**	81,23	**Pearlite %:** 72,30
Graphite main type (fixed):	VI		**JIS G 5502 Nodularity:**	78,64	**Ferrite %:** 15,05
Total rating (area%):					**Pores %:** 0,00

All graphite:			
Range (mic.)	**Size Class**	**Count**	**Area %**
> 1000	1	0	0
500 - 1000	2	0	0
250 - 500	3	3	1
120 - 250	4	37	7
60 - 120	5	190	63
30 - 60	6	82	26
15 - 30	7	89	2
0 - 15	8	70	1

All graphite mean Length:	42,55	µm
Corresponding Size Class:	6	
All graphite density:	91	1/mm
Count of all graphites:	471	
Nodules maximum Length:	120,83	µm
Corresponding Size Class:	4	
Nodules mean Length:	42,82	µm
Corresponding Size Class:	6	
Nodules density:	66	1/mm
Nodules count:	340	
Other types mean Length:	41,86	µm
Corresponding Size Class:	6	
Other types of graphite densit	25	1/mm
Other types of graphite count	131	

All Graphites:

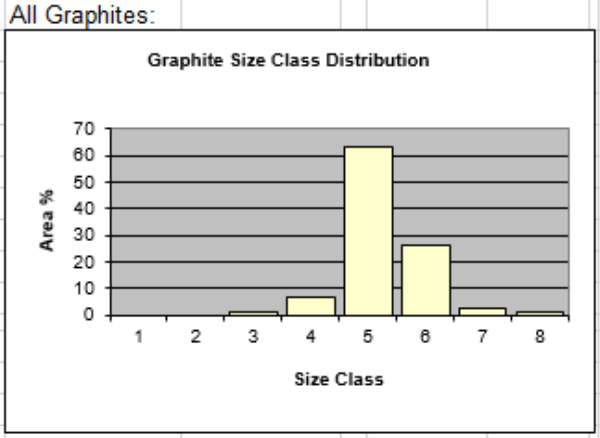

Nodules:

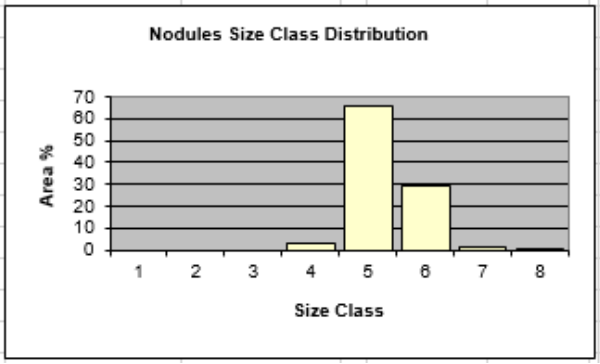

Figure3. 7: EN-GJS 500-7 microstructure with Nodule count(S.G iron):340 ferrite:15% pearlite:72% , graphite:12%

Sample ID:	GGG50-14		**Nodularity by Count:**	67,47	**Graphite %:** 4,25
Fields:	2		**Nodularity by Area:**	66,30	**Pearlite %:** 2,13
Graphite main type (fixed):	VI		**JIS G 5502 Nodularity:**	77,39	**Ferrite %:** 93,62
Total rating (area%):					**Pores %:** 0,00

All graphite:			
Range (mic.)	**Size Class**	**Count**	**Area %**
> 1000	1	0	0
500 - 1000	2	0	0
250 - 500	3	0	0
120 - 250	4	8	0
60 - 120	5	109	26
30 - 60	6	162	61
15 - 30	7	61	12
0 - 15	8	32	1

All graphite mean Length:	33,54	µm
Corresponding Size Class:	6	
All graphite density:	108	1/mm
Count of all graphites:	372	
Nodules maximum Length:	90,619	µm
Corresponding Size Class:	5	
Nodules mean Length:	30,65	µm
Corresponding Size Class:	6	
Nodules density:	73	1/mm
Nodules count:	251	
Other types mean Length:	39,55	µm
Corresponding Size Class:	6	
Other types of graphite density	35	1/mm
Other types of graphite count:	121	

All Graphites:

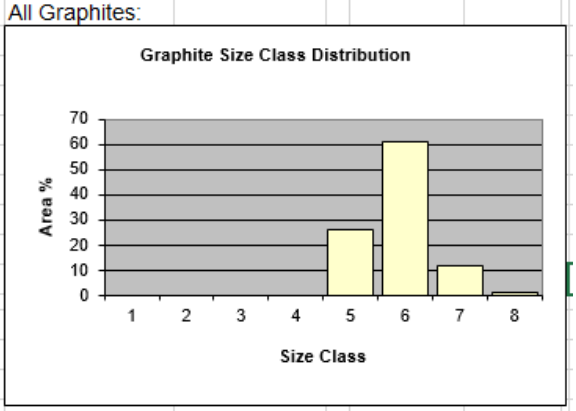

Nodules:

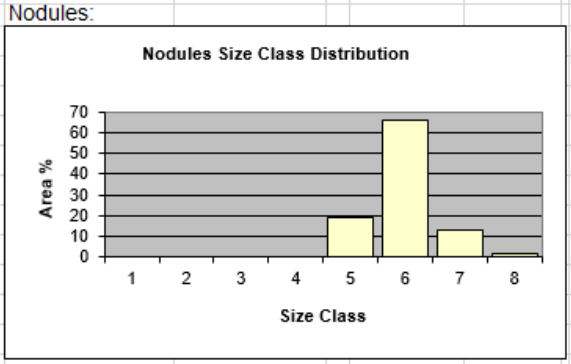

Figure3. 8: EN-GJS 500-14 microstructure with Nodule count (SSF): 251 ferrite:93.62% pearlite:2.13% graphite:4.25%

The nodule count of both alloys investigated is given above. The minimum required value for the specified area is 1 mmx1mm.

3.1.3 Mechanical results

The MTS three-ton tensile test machine was used according to the ASTM E8/E8M-09 Standard [23] to conduct and evaluate the stress-strain curves of materials. Below in figure 3.9, only one of six samples of stress-strain shows how the process

was carried out for all six samples of EN –GJS 500-7. Table 3.2 describes the values for the representative tensile test specimen.

Table3. 2: Tensile test sample dimension, length, and area values.

	Dimater (mm)	Area (mm^2)	Gauge Extensometer (mm)	Final length (mm)
Tensile Test Sample	14.160	157.4	70	78.06

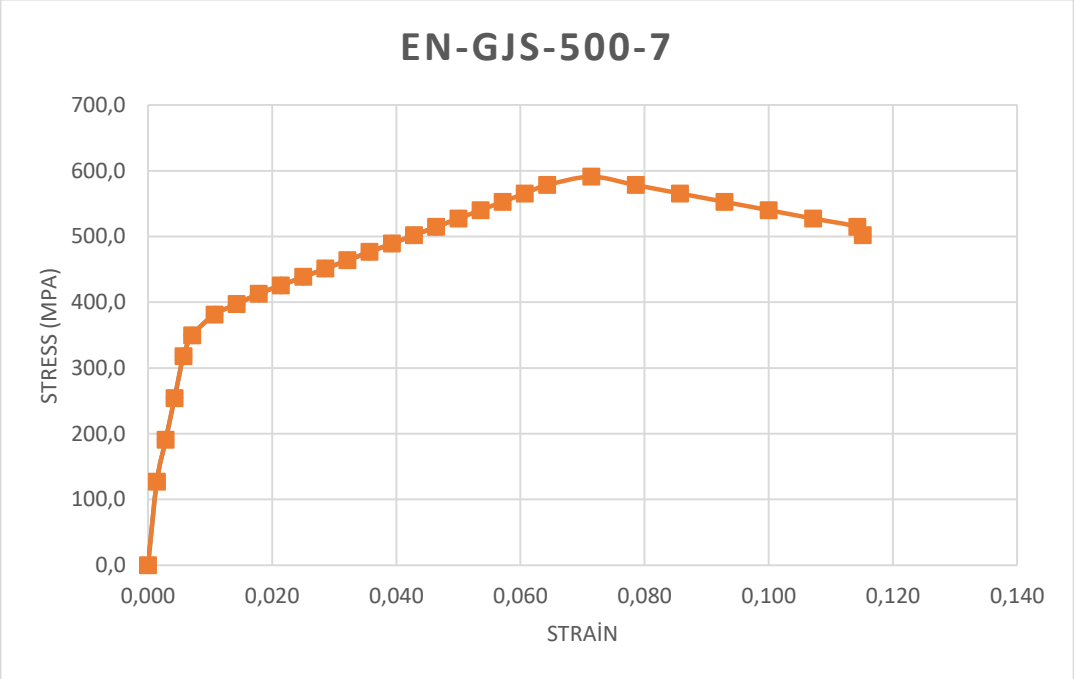

Figure3. 9: Stress-Strain curve for EN-GJS 500-7

In the figure3.9, the stress and strain values can be calculated employing the formula below also [22].

$\sigma = F/A\ (N/mm^2)$ and $\varepsilon = \Delta L/Lo$

Also, to compare the new generation with the old one, in figure 3.10, only one of six samples stress-strain is represented to show how the process was carried out for all six samples of EN –GJS 500-14. Table 3.3 describes the values for the representative tensile test specimen.

Table3. 3: Tensile test sample dimension, length, and area values.

	Dimater (mm)	Area (mm^2)	Gauge Extensometer (mm)	Final length (mm)
Tensile Test Sample	14.030	154.50	70	81.20

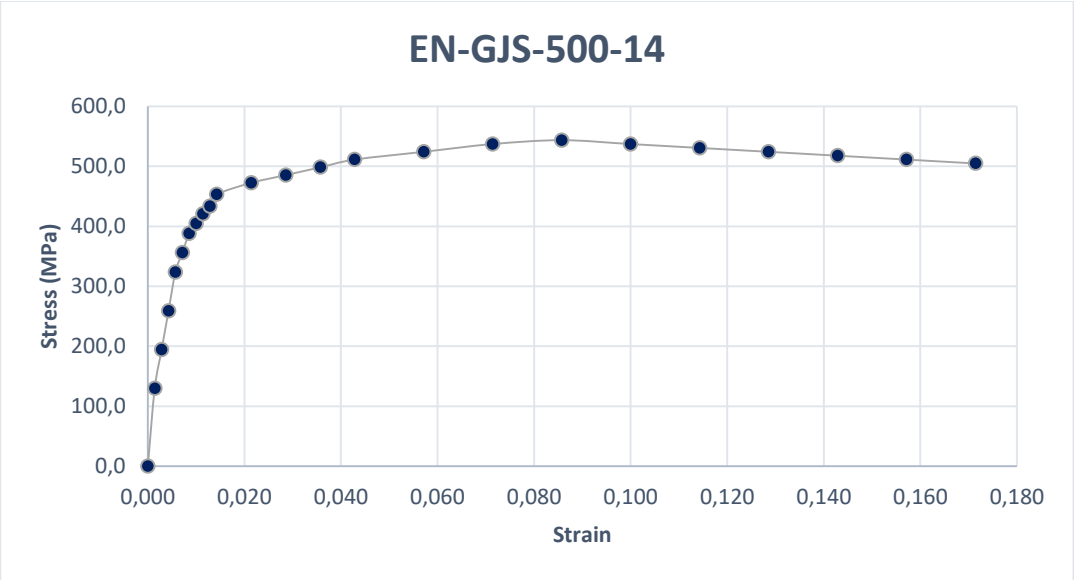

Figure3. 10: Stress-Strain curve for EN-GJS 500-14

In the figure3.10, the stress and strain values are calculated employing the formula below [22].

$\sigma = F/A\ (N/mm^2)$ and $\varepsilon = \Delta L/Lo$.

As mentioned, six samples from each material were prepared, and for all of them, the tensile test was applied, and the tensile test and hardness results are listed in the table below. Table 3.4 describes the EN-GJS500-7 mechanical tensile and hardness result of samples and Table 3.5 the EN-GJS 500-14 accordingly.

Table3. 4: Tensile test and hardness results of six specimens of EN-GJS 500-7 (S.G)

Test name	Tensile Strength (MPa)	Offset Yield Strength (MPa)	Max Load (KN)	Gauge Extensometer (mm)	Elongation (%)	Diameter (mm)	Hardness Values HB2
Test 1	578,2	324,290	88,365	70	10,875	13,950	197
Test 2	585,8	321,357	92,243	70	11,518	14,160	205
Test 3	570,7	320,071	85,490	70	10,986	13,810	183
Test 4	584,3	331,731	88,920	70	10,570	13,920	205
Test 5	578,2	331,181	92,088	70	9,521	14,240	196
Test 6	592,4	331,594	94,613	70	10,762	14,260	210
Average	581,6	326,704	90,286	70,0	10,705	14,057	199,3
standard Deviation	7,5	5,434	3,297		0,662	0,188	

Table3. 5: Tensile test and hardness results of six specimens of EN-GJS 500-14

Test name	Tensile Strength (MPa)	Offset Yield Strength (MPa)	Max Load (KN)	Gauge Extensometer (mm)	Elongation (%)	Diameter (mm)	Hardness Values HB2
Test 1	528,2	396,114	75,380	70	17,416	13,950	180
Test 2	516,8	407,854	70,721	70	19,975	14,000	176
Test 3	515,6	399,659	74,355	70	18,950	14,020	178
Test 4	512,0	407,985	68,271	70	18,735	13,960	175
Test 5	464,3	395,854	63,544	70	17,579	13,940	179
Test 6	539,7	409,254	73,854	70	18,729	13,980	184
Average	512,767	402,787	71,021	70,0	18,564	13,975	178,7
Standard Deviation	25,836	6,275	4,510		0,947	0,031	

The average values for the six specimens' tensile test, Yield strength, elongation, Brinell hardness, Nodule count, matrix ratio results are listed in table 3.6 and comparing accordance with EN 1563:2018 standard.

Table3. 6: Tensile test, hardness, and microstructure results of six specimen summaries.

Test Items	Tensile Strength MPa	Yield Strength MPa	Elongation %	Hardness value Brinell HB	Nodule count	Pearlite & Ferrite
Guidance value based on EN 1563: 2018 considering t≤30 mm for EN-GJS 500-7	500	320	7	170-230	-	Pearlitic 50-90
Average six specimen EN-GJS 500-7	581,6	326,7	10,7	199,3	340	Pearlite 72%
Guidance value based on EN 1563: 2018 considering t≤30 mm for EN-GJS 500-14	500	400	14	185-215	-	Ferritic Min 95
Average six specimen EN-GJS 500-7	512,7	402,78	18,73	178,7	251	Ferrite 95%

There is no reference to the Charpy impact test for EN-GJS 500-14 or new generation solid solution strengthened ferritic materials. Still, the results of 6 specimens carried out at room temperature are listed in Table 3.7 below. The test was carried out at room temperature with GALDABİNİ IMPACT 450 machine 10x10x55 mm dimension, and V type notched based on EN-1563:2018 standard [5].

Table3. 7: Charpy impact test for six samples EN-GJS 500-14 machined and prepared from U blocks.

Test item	Test sample set 1 (J)	Test sample set 2 (J)	Test sample set 3 (J)	Test sample set 4 (J)	Test sample set 5 (J)	Test sample set 6 (J)
Notched Impact Energy at RT	4.13	3.50	3.86	3.40	3.70	3.50

3.1.4 Thermal Analysis Results

The cooling behavior and effect of the Si on the cooling properties of these SSF cast iron alloys were examined for both EN-GJS500-7 and EN GJS 500-14 before and after with 0.5% FeSi inoculation cooling curves recorded using Quik-Cup and thermal analysis instrument by Electro-Nite Quick Cup. Figure 3.10 shows EN – GJS 500-7 before inoculation, and figure 3.11 shows the cooling curve of the same material after 0.5 % FeSi (0.75 % Si) inoculation.

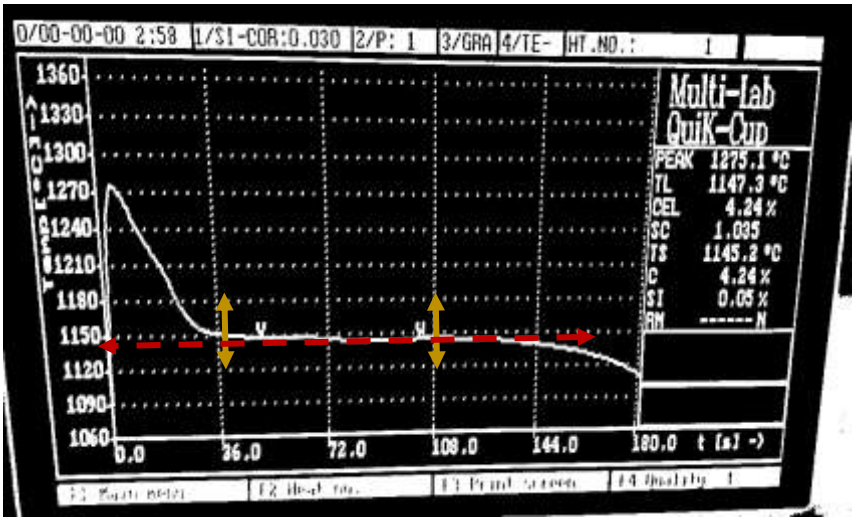

Figure3. 11: Thermal analysis of EN-GJS 500-7 before inoculation

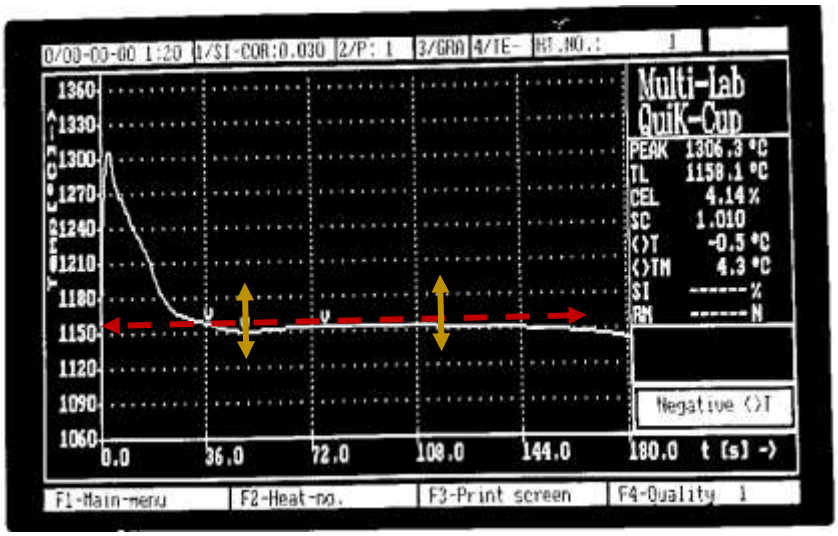

Figure3. 12: Thermal analysis of EN-GJS 500-7 after 0.5% FeSi inoculation

As marked on the graphs also, the time to reach maximum eutectic temp is 72 sec (108-36) before inoculation and 67 sec(43-110) after inoculation in the complete solidification time interval of the S.G iron alloy tested).

It can be seen that from Figure 3.12 after inoculation of EN-GJS 500-7 with 0.5%FeSi, the difference between theoretical eutectic (1152 °C) and maximum eutectic temp measured by thermal analysis(<>T) =ΔT change from 4.7 to -0.5 stands for the increase in eutectic temperature over 1152°C which is an evidence of fully graphite solidification. Liquidus temperature increased from 1147°C to 1158°C measured by thermal analysis. Additionally, to observe the cooling behavior of new generation materials, the thermal cooling behavior recorder also for EN-GJS 500-14. Below, Figure 3.13 shows EN-GJS 500-14 before inoculation, and figure 3.14 shows the cooling curve of the same material after 0.5 % FeSi (0.75 % Si) inoculation.

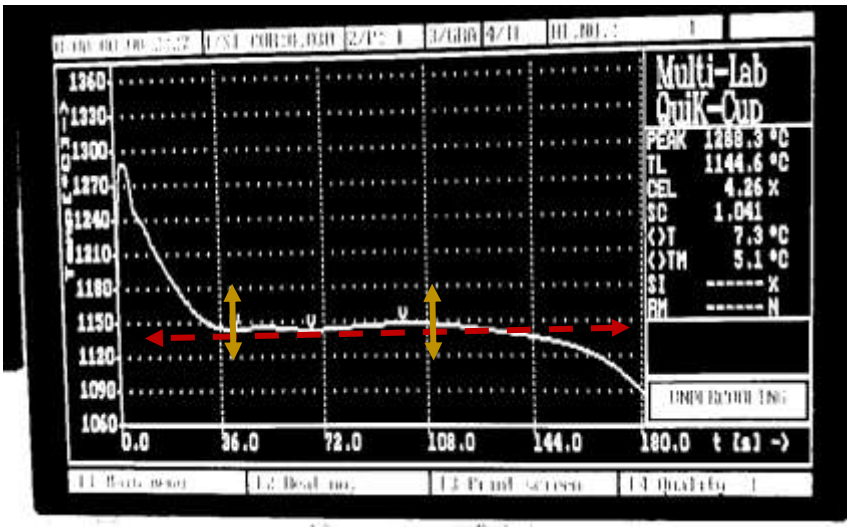

Figure3. 13: Thermal analysis of EN-GJS 500-14 before inoculation

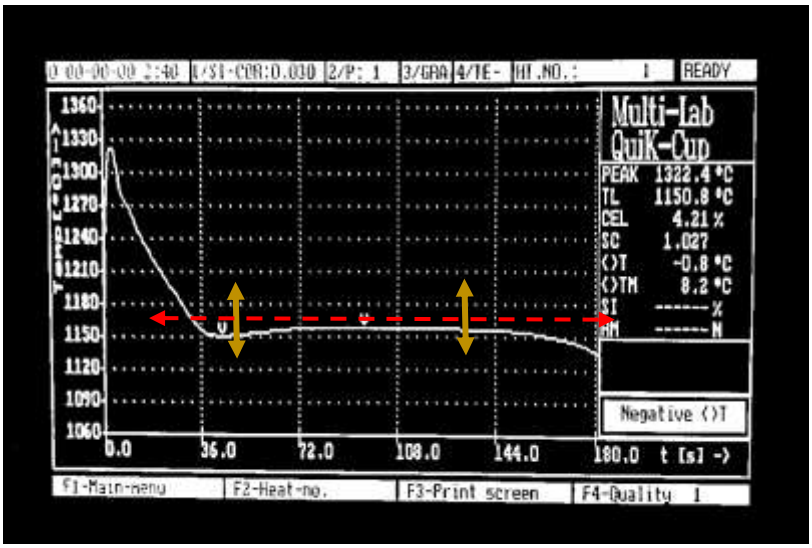

Figure3. 14: Thermal analysis of EN-GJS 500-14 after 0.5% FeSi inoculation

As marked on the graphs also, the time to reach maximum eutectic temp is 72 sec(108-36) before inoculation and 86 sec(130-44) after inoculation incomplete solidification time interval of SSF cast iron alloy).

It can be seen that from Figure 4.8 after inoculation of EN-GJS 500-14 with 0.5%FeSi, the difference between theoretical eutectic (1152°C) and maximum eutectic measured by thermal analysis(<>T) =ΔT change from 7.4 to -0.8 stands for the increase in eutectic temperature over 1153°C which is an evidence of fully graphite solidification. After Mg treatment with 0.5%, FeSi inoculation liquidus

temperature increased from 1144.6 0C to 1150.8 °C measured by thermal analysis. An increase in (<> T.M.) =ΔT_m stands for the difference between the maximum and minimum eutectic temperatures determined on the same cooling curve reveals the intensity of graphite formation due to inoculation.

CHAPTER 4

DISCUSSION

This study investigates the new generation nodular cast iron known as solid solution strengthened ferritic materials. New generation material following EN-1563:2018 standard is produced as EN-GJS 500-14 and old generation EN-GJS 500-7. New generation mechanical properties and microstructure are controlled by thermal analysis and cooling behavior. Comparing the first generation spheroidal cast iron EN-GJS 500-7 to the second generation spheroidal cast iron EN-GJS 500-14 in Table 3.1, alloying elements are different in wt% ratio as those have a different impact on microstructure. When figures 3.1 and 3.6 are examined, it is determined that the pearlite ratio of the EN-GJS-500-7 sample is high, and the ferrite ratio is low. The graphite morphology of both materials is mainly formed V and VI according to EN ISO 945-1. So for both materials in Figures 3.1 and 3.6, the microstructure mainly contains VI graphite type, which makes it possible to reach or fulfill the mechanical properties for ferritic and ferritic/pearlitic structure. Considering the number of nodules formed in the structure, those counted above the minimum requested one to obtain the desired mechanical and metallographic properties. In the EN-GJS-500-14 sample structure in Figure 3.6, the pearlite structure is seen in a small amount and seems so insignificant, and only the ferrite structure is located around the graphite spheres. Comparing these two microstructures, it can be concluded that silicon is a significant influencing factor on carbon equivalent levels, as it reduces carbon solubility in molten iron and promotes the formation of graphite rather than free carbide (cementite) during the cooling process up to the end of solidification. On the other hand, silicon lowers carbon solubility in solid iron, favoring carbon diffusion from austenite to existing graphite particles during the eutectoid process, promoting ferrite formation and

lowering pearlite concentration. The critical point that should be emphasized is that thanks to solid solution hardening, the material gets stronger without losing much of its elasticity and hardness until the silicon content of cast iron reaches around 4.3%. When the silicon amount is approximately 4.3% - 4.5%, we observe that the tensile strength and elongation values decrease with a larger slope, and the material becomes brittle. Moreover, silicon is such an element that tends to accumulate (segregate) around graphite nodules.

Therefore, although the total amount of Si in the alloy is below the critical amount since this element accumulates around the graphite nodules, it can concentrate locally in these regions and cause the sphere environment to become brittle. Table 3.6 shows the mechanical test results for tensile and hardness of spheroidal graphite cast irons for both first and new-generation samples.

Considering the new generation EN-GJS 500-14, although only 5% pearlite structure is observed in the microstructure, the yield strength and elongation value are greater than the other old generation samples.

Considering both materials' cooling behavior, the thermal analysis provides to control or observes the CEL and the TL. of composition. In nodular cast iron, it is important to arrange a composition like a hypo eutectic rather than eutectic or hyper eutectic. The reason is that, during eutectic of hyper eutectic solidification, when graphite nodules nucleate, passing the time, those graphite’s grow and cause some known defect as shrinkage inside the mould.

However, if the composition is hypo eutectic, primary formed austenite dendrites restrain the formation of shrinkage in the mould. As a result of this mean of thermal analysis, it is possible to control the cooling behavior in Figures 3.12 and 3.14, where the composition is hypo eutectic. In other words, employing liquidus temperature TL. in thermal analysis ensures that the produced composition is below eutectic temperature (hypo eutectic); otherwise, if the composition is not as desired, observing the TL. will be impossible during solidification for eutectic or hyper eutectic composition.

Furthermore, Thermal analysis reveals that after Mg treatment with 0.5% FeSi (75%Si) inoculation, the liquidus temperature increases for both materials. So it means that the intensity of graphite production results from inoculation and negative undercooling cause fully graphitic solidification. For both materials, ΔT or undercooling amounts between TEmin and TEmax are investigated, and a decrease of ΔT after inoculation is observed as expected.

It is observed that both Si-content and inoculation operate as beneficial influencing variables, increasing representative temperatures and lowering undercooling degrees for the eutectic reaction and after solidification.

CHAPTER 5

CONCLUSIONS

The tensile strength of DI iron alloys produced in this work was slightly higher due to the presence of higher pearlite than SSF alloys. There is a considerable increase in elongation and yield strength in SSF alloy compared to DI. The time to reach maximum eutectic temp in SSF materials was measured as higher than DI after inoculation because of the graphite precipitation stage. After inoculation with 0.5% FeSi, the increase in liquidus temperature for DI was determined to be higher than for SSF because of recoalescence due to more graphite formation in DI alloys.

The cooling curve of SSF cast iron revealed that there is no increase due to graphite formation in a narrow time interval, but it is parallel to the time axes without clear recoalesence during eutectic transformation. Therefore, there is no graphite accumulation in the matrix related to the extended time interval during solidification containing graphite nucleation in the eutectic transformation range. It was correlated to extended graphite formation with little recoalesence, which is evidence of no probability of shrinkage. The time to reach maximum eutectic temp was 72 sec before inoculation. This is the same in both SSF and S.G alloys, but after inoculation, during the graphite precipitation stage, this time interval is 67 sec for S.G iron and 86 sec for SSF alloys which is longer than the time for graphite formation in S.G iron.

After Mg treatment with 0.5%, FeSi inoculation liquidus temperature increased for both SSF and S.G alloy measured by thermal analysis. This is evidence of higher recoalescence due to more graphite formation in S.G alloys.

REFERENCES

[1] ASM Handbooks Online, Volume 3: Alloy Phase Diagrams. ASM International, 2012, available (accessed on 22.10.2015): http://products.asminternational.org/hbk/index.jsp.

[2] C. Labreque and M. Gagne, "Ductile iron: Fifty years of continuous development," Canadian Metallurgical Quarterly, vol. 37, 1998

[3] Okunnu, Rilwan. "High Strength Solution-Strengthened Ferritic Ductile Cast Iron." Aaltodoc, 24 Aug. 2015, http://aaltodoc.aalto.fi/handle/123456789/17814.

[4] EN ISO 945, microstructure of cast irons - Part 1: Graphite classification by visual analysis," Finnish Standards Association, Helsinki, 2008, 19 p.

[5] Standard E. NORM EN 1563:2018, founding - spheroidal graphite cast irons. EUROPEAN COMMITTEE FOR STANDARDIZATION. 2011;ICS 77.080.10.

[6] Arda Çetin, "Dökümcünün El Kitabı: Küresel Grafitli Dökme demir " (2019, November 11). Sayı 1, 2016, http://Dokumhane.net.

[7] DIN EN 1564:2012-01, Founding - Ausferritic nodular cast iron; German version en_1564:2011. (n.d.). doi:10.31030/1799654

[8] ASM Handbooks Online, Volume 15: Castings. ASM International, 2008, available (accessed on 2.11.2015): http://products.asminternational.org/hbk/index.jsp.

[9] ASM Handbooks Online, Volume 1: Properties and Selection: Irons, Steels, and High-Performance Alloys. ASM International, 2014, available (accessed on 29.10.2015): http://products.asminternational.org/hbk/index.jsp.

[10] G. M. Goodrich, Ed., Iron Castings Engineering Handbook. American Foundry Society, 2006.

[11] Encyclopedia of Materials: Science and Technology. Elsevier Ltd, 2001, pp. 1003-1011.

[12] Alhussein, Akram, et al. "Influence of Silicon and Addition Elements on the Mechanical Behavior of Ferritic Ductile Cast Iron." A, 10 Mar. 2016, https://www.academia.edu/23043213/Influence_of_silicon_and_addition_elements_on_the_mechanical_behavior_of_ferritic_ductile_cast_iron.

[13] Partanen, O. (2016). Optimization of solid solution strengthened ferritic ductile iron production by thermal analysis and solidification simulation. Master's Thesis ,Tampere University of Technology.

[14] Stets, W., Löblich, H., Gassner, G., & Schumacher, P. (2014). Solution strengthened ferritic ductile cast iron properties, production and application. International Journal of Metalcasting, 8(2), 35-40. doi:10.1007/bf03355580

[15] Lin, Hung-Mao, et al. "Effect of Silicon Content on Intergranular Embrittlement of Ferritic Spheroidal Graphite Cast Iron Suffered from Cyclic Heating." MATERIALS TRANSACTIONS, The Japan Institute of Metals and Materials, 6 Sept. 2005, https://www.jstage.jst.go.jp/article/matertrans/44/1/44_1_173/_article.

[16] Glavas, Z., Strkalj, A., & Stojakovic, A. (2016). The properties of silicon alloyed ferritic ductile irons. The Properties of Silicon Alloyed Ferritic Ductile Irons, 55(METABK), 293.

[17] Schlussbericht Werkstoff- und Fertigungstechnische Grundlagen der Herstellung und Anwendung von hoch Silizium-haltigen Gusseiesen mit Kugelgraphit. (2010, July 30). Retrieved June 30, 2012.

[18] Serrallach, J., Lacaze, J., Sertucha, J., Suárez, R., & Monzón, A. (2010). Effect of selected alloying elements on mechanical properties of pearlitic nodular cast irons. Key Engineering Materials, 457, 361-366. doi:10.4028/www.scientific.net/kem.457.361

[19] Duit B. EN 1563: New generation ductile irons (solid solution strengthened ductile irons). . 2012.

[20] Ishikawa, K., & Tsuya, K. (1977). Mechanical properties of new High Strength Ferritic Iron Alloy for Cryogenic Service. Cryogenics, 17(5), 295-297. doi:10.1016/0011-2275(77)90199-0

[21] Stan, I., Anca, D., Stan, S., & Riposan, I. (2021). Solidification pattern of si-alloyed, inoculated ductile cast irons, evaluated by thermal analysis. Metals, 11(5), 846. doi:10.3390/met11050846

[22] Callister, W. D., & Rethwisch, D. G. (2020). Materials science and engineering. Hoboken, NJ: Wiley.

[23] ASTM E8/E8M-09, Standard Test Methods for Tension Testing of Metallic Materials; ASTM International: West Conshohocken, PA, USA, 2009

[24] E. Autere, Y. Ingman, and P. Tennilä, Valimotekniikka. Insinööritieto Oy, 1986.

[25] Gonzaga, R. A., & Carrasquilla, J. F. (2005). Influence of an appropriate balance of the alloying elements on microstructure and on mechanical properties of nodular cast iron. Journal of Materials Processing Technology, 162-163, 293-297. doi:10.1016/j.jmatprotec.2005.02.040

[26] D. Stefanescu, "Thermal analysis – theory and applications in metalcasting," International Journal of Metalcasting, vol. 9, 2015.

[27] H. Nakae, S. Jung, and H.-C. Shin, "Formation mechanism of chunky graphite and its preventive measures," Journal of Materials Science and Technology, vol. 24, pp. 289–295, 2008.

[28] Article sulphur and oxygen effects on high-si ductile iron ... (n.d.). Retrieved February 2, 2022, from https://www.researchgate.net/publication/342547218_Sulfur_and_Oxygen_Effects_on_HighSi_Ductile_Iron_Casting_Skin_Formation/fulltext/5efaaa3d299bf18816f36170/Sulfur-and-Oxygen-Effects-on-High-Si-Ductile-Iron-Casting-Skin-Formation.pdf

[29] DIN EN ISO 6892-1:2019-10, Metallische Werkstoffe_- Zugversuch_-teil_1: Prüfverfahren bei raumtemperatur (ISO/FDIS_6892-1:2019); Deutsche und Englische Fassung pren_iso_6892-1:2019. (n.d.). doi:10.31030/3064700